Journal of Hydrology: Regional Studies 65 (2026) 103473

Contents lists available at ScienceDirect

Journal of Hydrology: Regional Studies

journal homepage: www.elsevier.com/locate/ejrh

Multiparameter approach to evaluate spatiotemporal hydrochemical variations at different scales: Improved understanding of the deep Brilon karst system

Alexander Kaltenbrunn [a,*], Nadine Goeppert [b], Nico Goldscheider [a]

[a] Institute of Applied Geosciences, Division of Hydrogeology, Karlsruhe Institute of Technology (KIT), Kaiserstr. 12, Karlsruhe 76131, Germany
[b] Institute of Geological Sciences, Division of Hydrogeology, Free University Berlin, Malteserstr. 74-100, Berlin 12249, Germany

ARTICLE INFO

Keywords:
Karst aquifer
Hydrochemistry
Spatiotemporal variations
Trace elements
Rare-earth elements
Germany

ABSTRACT

Study region: The Brilon karst system (Germany), crucial for the drinking water supply of the region.
Study focus: The study provides the first comprehensive evaluation of hydrochemical data from the karst system. To cover both spring and catchment scale, sampling sites include springs, drinking water wells, groundwater monitoring wells, and surface streams. In addition to publicly available data, six sampling campaigns were realized over an annual cycle. Physicochemical data, major ions, trace elements, and rare-earth elements were evaluated using ion ratios, multivariate statistics, seasonal and long-term trends to develop a hydrogeological conceptual model.
New hydrological insights for the region: Results show strong spatial variations at spring and catchment scale, while seasonal variations are low. The karst system is predominantly controlled by deeper groundwater, which is characterized by higher Na^+ and Cl^- concentrations, and enriched with the trace elements Li, Rb, Sr, Cs, U, Ba, and Ti. Ion ratios of 0.86 for Na^+/Cl^- and 45.9 for Na^+/K^+ show that the deeper karst groundwater is related to the dissolution of evaporites. A waste water influenced sinking stream has a Na^+/Cl^- ratio of 1 related to the application of road salt. It is further characterized by higher NO_3^- and K^+ concentrations, and shows a positive gadolinium anomaly. At drinking water abstraction sites, long-term trends show significantly increasing Na^+ and Cl^- concentrations, while NO_3^- concentrations are decreasing or stable.

1. Introduction

Karst aquifers are among the most important sources of water worldwide and provide drinking water for about 9.2 % of the global population (Stevanović, 2019). Karst systems are thus of great economic importance for water management authorities. At the same time, they are some of the most complex and difficult systems to decipher (Bonacci, 2015), and play a special role in hydrological research. Due to their particularities, they show unique and complex hydraulic properties (Bakalowicz, 2005; Ghasemizadeh et al., 2012) and are characterized by inherently complex groundwater flow systems (Toth and Katz, 2006). Numerous karst features provide a direct and rapid hydraulic connection between surface waters and groundwater (Bonacci, 2015), making them particularly vulnerable to contamination (Zwahlen, 2004). The pronounced spatial heterogeneity of karst aquifers and the temporal variability of

* Corresponding author.
E-mail address: alexander.kaltenbrunn@kit.edu (A. Kaltenbrunn).

https://doi.org/10.1016/j.ejrh.2026.103473
Received 6 February 2026; Received in revised form 19 April 2026; Accepted 20 April 2026
Available online 1 May 2026

karst groundwater pose general problems for research and require specific investigation methods (Goldscheider et al., 2007). Hydrochemical investigations are among the most used techniques to characterize karst aquifers (Haryono, 2023). They not only provide information about water quality, but also give insight into the functioning of karst aquifers (Hunkeler and Mudry, 2007). Research of hydrogeochemical processes are critical to obtain information for a sustainable use and protection of karst groundwater (Wu et al., 2020; Milanović and Vasić, 2015).

A combination of major ion and trace element data provides valuable information on the origin of waters and on fluid-rock interactions, and can significantly enhance the understanding of an aquifer (Göb et al., 2013; Guo et al., 2025). Former studies showed that detailed hydrochemical evaluations are suitable to improve the understanding and to develop conceptual models of the investigated systems in different geological and hydrological settings (e.g. Carucci et al., 2012; Kpegli et al., 2018; Gil-Márquez et al., 2019; Wang et al., 2024). Karst aquifers located in humid and temperate climate zones are often rich in groundwater reserves (Stevanović et al., 2024), this applies especially for deep karst systems. In the context of climate change with increasing water scarcity, deep karst groundwater is an important resource (Gong et al., 2025). The use of deep karst groundwater resources for drinking water supply offers advantages over shallow karst groundwater. Larger water storage capacities facilitate a sustainable water management, particularly in dry periods, and contamination risk from the surface can be less pronounced. Therefore, the importance of deep karst aquifers for research and water management authorities is likely to increase in the future.

However, compared with typical shallow karst systems, less research dealing with deep carbonate systems is available (e.g. Toth and Katz, 2006; Black, 2012; Stober, 2014; Gong et al., 2025). In these systems, hydrological events can be buffered due to larger storage capacities, resulting in slower reaction times. Due to deep flow paths, longer residence times, and water-rock interactions, deep karst groundwater can exhibit particular hydrochemical characteristics. Karst water that was in contact with evaporites often shows high sulfate concentrations (Bao et al., 2022; Kuniansky et al., 2022), is enriched with trace elements, and sometimes also has high sodium and chloride concentrations (Hunkeler and Mudry, 2007).

The Brilon karst system (BKS) in Germany is an example of a deep carbonate aquifer and is used for the drinking water supply of 26,000 people. Typical problems of karst research apply to this area. The high-purity Brilon reef limestone is extracted at several large quarries, leading to conflicts of use between water management authorities and the raw materials industry. On the one hand, the karstified limestone provides a significant water reservoir for the drinking water supply, on the other hand the pure limestone is sought-after by the raw materials industry. Consequently, the Brilon reef limestone is both a reservoir and a resource. To date, very few hydrochemical research was carried out in the complex BKS. Former research in the 1940s and 1970s was restricted to the main karst spring draining the system, the Alme springs (AS). AS consists of more than 100 individual orifices forming a spring pond. Main findings of former studies are summed up in Koch and Vogel (1992) and Koch (1998) who state a quite similar water chemistry at AS. Only for sodium and chloride, spatial variations were observed for the individual orifices, with chloride concentrations varying between < 45 and > 100 mg/L. Hence it was possible to delimit chloride concentration zones at AS. Koch (1998) relates the salt with older karst groundwater from deeper parts of the aquifer. A mean residence time of 30–50 years was found for the older karst groundwater by means of ^{14}C dating technique. The origin of the salt is unknown, as there are no halite rocks in the area. It is assumed that it stems from water entering the BKS via fault structures in greater depths.

These findings indicate strong spatial variations within the BKS, even at spring scale. But sampling was restricted to AS, and only major ions and physicochemical properties were measured, which points out the need for more detailed investigations. Some factors make a hydrochemical approach particularly suitable for the Brilon area. Data from drinking water wells (DWW) and groundwater monitoring wells (GMW) spread over the catchment area are publicly available, including long-term data starting in 1976. Data from sinking streams, including a waste water influenced stream (WWIS) are also available. To expand the dataset with regard to sampling sites and parameters, six sampling campaigns were carried out over an annual cycle for this study. Measured parameters include physicochemical properties, major ions, trace and rare-earth elements (REE). A compilation of the datasets allowed to thoroughly evaluate the water chemistry at both spring and catchment scale. Samples from WWIS and sinking streams allow to identify anthropogenic contamination influencing the BKS from the surface and to compare them with characteristics of the deeper karst groundwater.

To ensure a sustainable drinking water supply of the region, an improved understanding of the complex hydrogeology of the BKS is essential. This is the first comprehensive international study describing the hydrochemistry of this deep and important karst groundwater flow system. The general objective is to deepen the understanding of the functioning of the system and to develop a hydrogeological conceptual model. The following specific research objectives are defined:

(1) Systematically investigate the spatial hydrochemical variations at spring and catchment scale, and identify possible differences between sampling site types.
(2) Identify and compare the origin of the sodium and chloride concentrations in the deeper groundwater and in the WWIS. Determine correlations of Cl^- with other parameters.
(3) Evaluate seasonal variations over an annual cycle, and identify the impact of the WWIS and surface streams sinking into the BKS.
(4) Identify hydrochemical long-term trends and elucidate implications for the drinking water supply.

2. Study area

Fig. 1a shows the location of the BKS in the central part of Germany within the state of North Rhine-Westphalia (NRW). The karst system is set in the massive Brilon reef limestone complex, which developed from the Middle to Late Devonian (Heuer et al., 2015), and

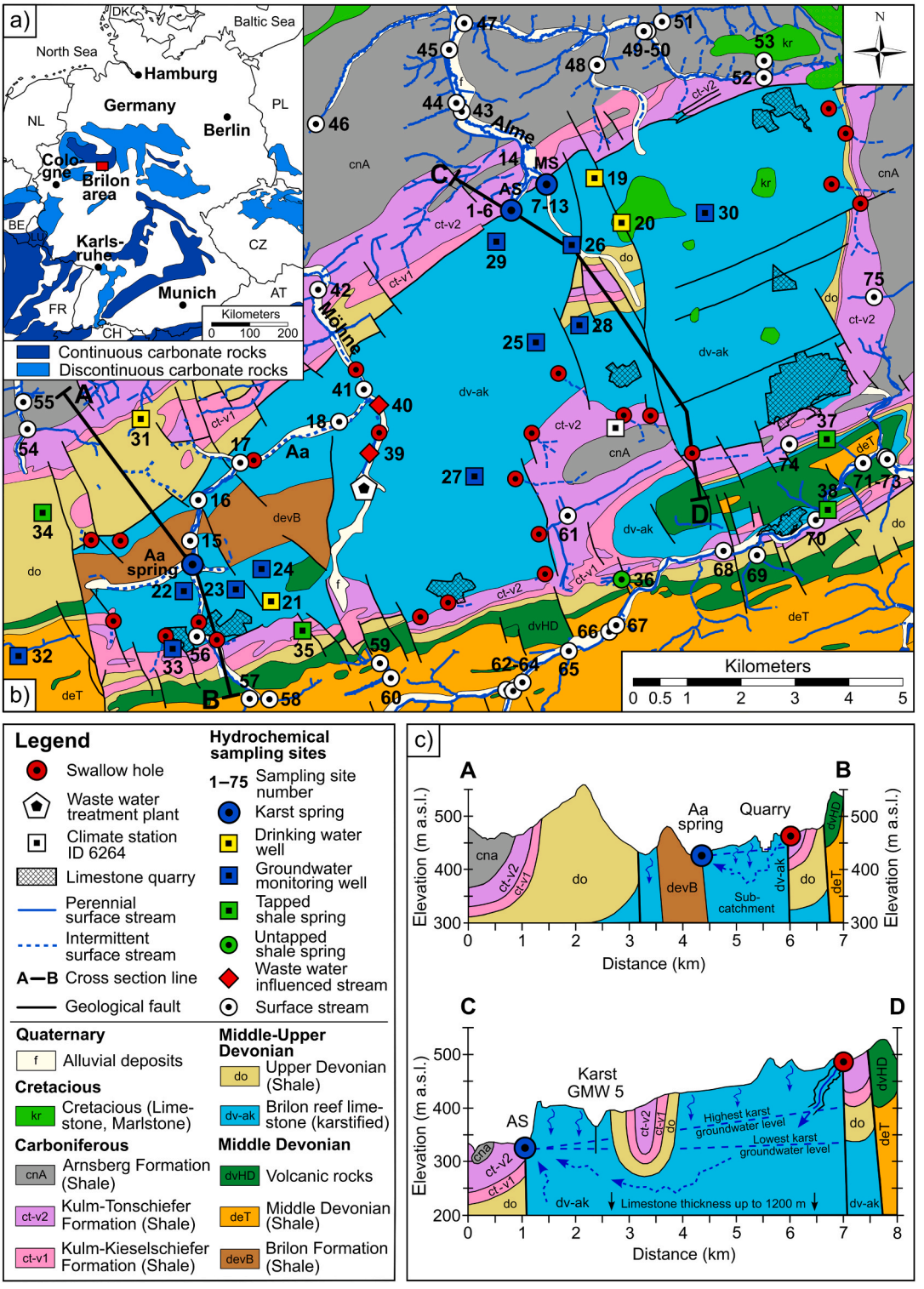

Fig. 1. Study area. a) Excerpt from WOKAM (Chen et al., 2017), the Brilon area is marked with a red rectangle. b) Simplified geological map of the Brilon karst system with hydrochemical sampling sites. Base map: Modified after Geological Service NRW (2024). c) Generalized geological cross sections of the Brilon reef limestone complex, 10x vertically exaggerated.

is one of the first studied and most investigated Middle Devonian reef complexes throughout the world (Pas et al., 2013). In the center of the Brilon Anticline, shales from the Brilon Formation are exposed at the land surface, dividing the reef limestone in a northern and a southern part (Fig. 1b). Two generalized geological cross sections of the Brilon area are shown in Fig. 1 c. A geological drilling program

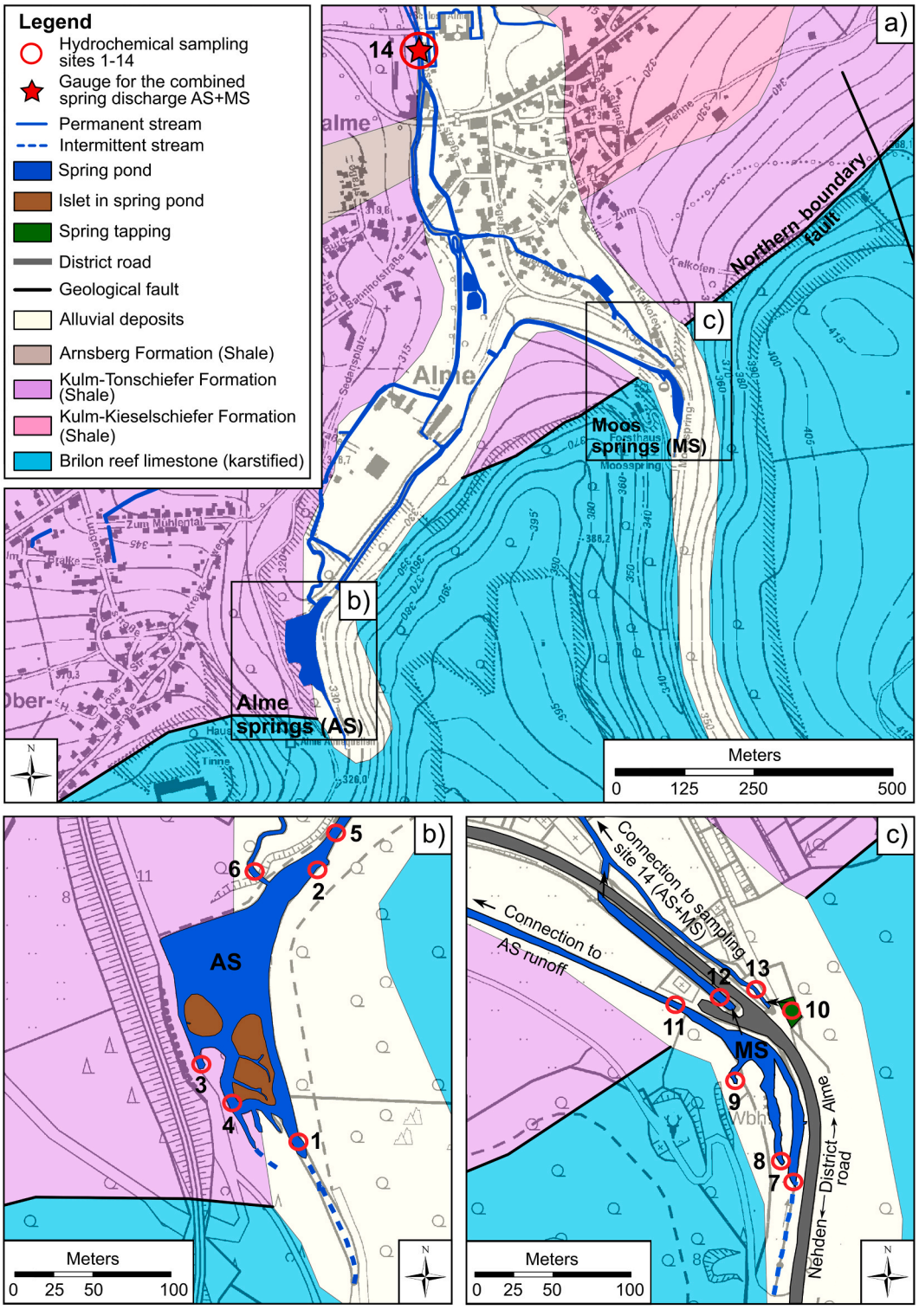

Fig. 2. Map of the karst springs AS and MS. a) Location of AS and MS with the gauge for the combined spring discharge, sampling site 14. b) Map of AS with sampling sites 1–6. c) Map of MS with sampling sites 7–13. Base maps: Geological Service NRW (2024); Bezirksregierung Köln (2024a,b).

was carried out in the 1970s by the German Federal Institute for Geosciences and Natural Resources. Although the deepest borehole reached down to 919 m below ground, the lower limit of the reef limestone was not encountered. The maximum thickness is therefore generally assumed to be at least around 1000 m, Stichling et al. (2022) state a maximum thickness of 1200 m. At the southern and eastern margin, a number of swallow holes drain the water from sinking streams coming from allogenic shale areas into the BKS (Fig. 1b). The Brilon area is extensively used for agriculture, only small parts in the northeast are forested.

The hydraulically low permeable shales of the Brilon Formation separate the BKS into a main catchment and a subcatchment. The latter is drained by the Aa spring, feeding the Aa surface stream (Fig. 1b,c). Starting from the confluence of Aa and WWIS this surface stream is named Möhne. Interconnection of the catchments is provided via swallow holes in Aa and Möhne (Fig. 1b). Two nearby karst springs drain the main catchment at an elevation of 320 m above sea level (a.s.l.), the Alme springs (AS) and Moos springs (MS). They are located at the northern boundary fault and are only 800 m apart (Fig. 2a). AS consists of more than 100 individual orifices forming the Alme spring pond (Fig. 2b). Most of the individual orifices are located below the pond's water table, and are therefore not directly accessible for sampling. The MS area is much smaller but similarly structured with several individual outlets (Fig. 2c). AS and MS feed the Alme river.

3. Materials and methods

3.1. Data acquisition and sampling sites

Data from different sources were compiled for this study. Six sampling campaigns were carried out over an annual cycle from September 2020 to July 2021 at 26 relevant sampling sites distributed throughout the BKS and its surroundings. Locations of sampling sites 1–4 at AS were selected to cover the four chloride concentration zones as given in Koch and Vogel (1992). Time periods of the sampling campaigns are shown in Section 4.4 (Fig. 10) and in Table S1 in the electronic supplementary material.

The measurement program included physicochemical parameters (water temperature, specific electrical conductivity (EC), dissolved oxygen (DO), pH), total organic carbon (TOC), dissolved organic carbon (DOC), major ions (Ca^{2+}, Mg^{2+}, Na^{+}, K^{+}, HCO_3^-, Cl^-, NO_3^-, SO_4^{2-}), trace elements (Li, Be, Al, V, Cr, Mn, Fe, Co, Ni, Cu, Ga, As, Rb, Sr, Cd, Cs, Ba, Ti, Bi, U, Th), and REE (La, Ce, Pr, Nd, Sm, Eu, Gd, Tb, Dy, Ho, Er, Tm, Yb, Lu). Physicochemical parameters were directly measured in the field at the sampling sites, laboratory analyses were conducted shortly after sampling in the hydrogeology laboratory at KIT. Anions were measured by means of ion chromatography. Cations, trace elements and REE were determined by means of inductively coupled plasma mass spectrometry. TOC and DOC were measured by oxidative combustion and subsequent determination of carbon dioxide. To quantify HCO_3^-, acid capacity to pH 4.3 was measured with a titrimetric Alkalinity test. The data collected during the six sampling campaigns is available via a HydroShare repository (Kaltenbrunn et al., 2026).

For sampling sites managed by the state of NRW, hydrochemical data are publicly available via the dataset OpenGeodata.NRW (2025a) for groundwater sampling sites, and the dataset OpenGeodata.NRW (2025b) for surface streams. Discharge measurements of AS+MS at sampling site 14 were obtained from the dataset OpenGeodata.NRW (2025c). Further information on accessing the OpenGeodata.NRW datasets is given in the electronic supplementary materials S2-S5. Daily precipitation and air temperature data (climate station ID 6264) were obtained from the German Meteorological Service (2026). Furthermore, the Brilon municipal utilities provided hydrochemical data from their drinking water abstraction sites.

Compiling the datasets resulted in a total of 2207 water samples from 75 sampling sites, shown in Fig. 1b (catchment scale) and Fig. 2 (spring scale). To emphasize the hydrochemical particularities of the BKS and to delimit the karst water chemistry from other water types, sampling sites located in the surrounding shale areas not contributing to the BKS were included in the study. Coordinates, naming, sampling groups, sampling periods, and data sources for each sampling site are provided in Table S6 and in the .kmz file in the electronic supplementary material. Sampling sites were classified in eleven groups, distinguishing between karst springs, drinking water wells (DWW), groundwater monitoring wells (GMW), shale groundwater, the waste water influenced stream (WWIS), and surface streams. The groups with corresponding sampling site numbers are given in Table 1 in Section 4.1, locations are shown via the sampling site numbers in Fig. 1b. Karst water is represented by sampling sites 1–30. Note that sampling sites 15–18 (Aa spring/stream), 21 (Karst DWW 3), and 22–24 (Karst GMW 1–3) are located in the subcatchment in the southwest of the Brilon reef limestone. The location of the subcatchment is depicted in the cross-section A-B in Fig. 1c. Waste water treatment plant (WWTP) effluents sink into the BKS via swallow holes, they are sampled at sites 39 and 40 (WWIS 1 and 2). In Fig. 5 both the sampling site numbers and names are shown together giving an overview on the locations of the most relevant sampling sites.

3.2. Data processing and evaluations

Due to the different data sources, measured parameters and sampling time periods are very individual for each sampling site. Units of concentrations were equalized and measurements were checked for completeness and plausibility. Eventually, the dataset was filtered for samples with complete data for the eight major ions. Ion balances were calculated according to DIN 38402–62 (2014), all samples with an ion balance error > 5.0 % were excluded from the dataset. Only for the long-term trends, all available major ions data were used. Total dissolved solids (TDS) were calculated as sum of the major ions. After data filtering, 455 samples from 40 sampling sites remained for the evaluation of the major ions. For all further sampling sites, only physicochemical properties could be considered for the evaluations. Since relevant trace elements and REE data are rarely found in the OpenGeodata.NRW datasets, it was decided to only use the homogeneous measurements from the authors' sampling campaigns in 2020–2021 for these parameters. All evaluations, data plotting, and statistical analyses were performed with the software OriginPro, version 2025b (OriginLab Corporation), maps were

created with ArcGIS Pro 3.5.4 (Esri Inc.).

3.2.1. Origin of sodium and chloride and correlations with other parameters

Ion ratios are commonly used to evaluate the origin of waters, for this study ratios were calculated from equivalent concentrations. Calcite dissolution results in a Ca^{2+}/HCO_3^- ratio of 1, salinity sources are identified by the Na^+/Cl^- ratio. Dissolution of the mineral halite results in a Na^+/Cl^- ratio of 1 (Alijani et al., 2025; Bao et al., 2022), whereas seawater has a ratio of 0.86 (Möller, 1990; Bauer et al., 2022). Furthermore, data of the standard seawater composition were compiled from Nordstrom et al. (1979), Drever (1997), and Hölting and Coldewey (2019) to calculate ratios of Na^+/Mg^{2+} (= 4.42), Na^+/K^+ (= 45.9), and Ca^{2+}/HCO_3^- (= 8.8). Cl^- is a chemically very stable ion and acts as a conservative tracer in natural environments (Jones et al., 1999; Subyani and Şen, 2006). In order to explore the correlations of Cl^- with further parameters, a nonparametric Spearman rank correlation test was applied for the 2020–2021 data with a significance level of 95 % (p-value = 0.05). Bi and Th were excluded as too much values below the detection limit occur for these parameters. Only significant (p-value < 0.05) and positive or negative correlations > 0.45 were considered. For the rank correlation test, sampling sites 1–14 (AS and MS), and 19–21 (Karst DWW 1–3) were used representative for the karst groundwater group. For the surface streams group, sampling sites 16, 17, 39, 48, 49, 51, 52, 56, and 61 were used, as the further sampling sites were not sampled during the 2020–2021 campaigns.

3.2.2. Seasonal and long-term trends

A hydrograph of AS+MS, groundwater levels, and chemographs of Cl^- and NO_3^- are shown to compare variations of surface water and karst water over the course of the six sampling campaigns. AS 5 (sampling site 5) and MS 5 (sampling site 11) are shown as they are considered to be most representative for the two karst springs. Surface stream 16 (sampling site 61) sinks into the BKS at a swallow hole (Fig. 1b). Thus, to evaluate impacts from the surface, WWIS 1 and Surface stream 16 are shown. Evaluation of long-term data was applied using linear trends with a significance level of 95 % (p-value = 0.05). Acid capacity to pH 4.3 (HCO_3^-) is often missing in the older long-term data, thus ion balances couldn't be calculated. As the long-term data are important for a better understanding of the BKS, these data were used regardless of the missing ion balance checking, and all available major ions data were used to cover the long-term scale.

3.2.3. Normalization of REE data

Normalization of REE data allows to detect anomalies (Bau et al., 2018), and is useful to delineate groundwater flow systems (Johannesson et al., 1997). Effluents from WWTPs typically show an anthropogenic gadolinium (Gd) anomaly. Gd is used in contrast agents for magnetic resonance imaging since the late 1980s. After excretion from the patient's body it is washed to WWTPs via the sewerage system (Schmidt et al., 2019; Boester and Rüde, 2020), and increasing Gd concentrations are recorded in water resources (Tepe et al., 2014; Ebrahimi and Barbieri, 2019). Therefore, temporal variations of Gd concentrations can be used to better understand the interactions between surface water and groundwater (Brünjes and Hofmann, 2020; Pujades-Garnes et al., 2025). For this study, REE data from the 2020–2021 sampling campaigns were normalized to Post Archean Australian Shales (PAAS) after McLennan (2001).

3.2.4. Multivariate statistics

Multivariate statistics require normally distributed data. As most of the hydrochemical parameters are not normally distributed, a z-score normalization of the dataset was carried out prior to multivariate statistics according to Eq. (1):

$$z_i = \frac{x_i - \overline{x}}{s} \tag{1}$$

with z_i = standard score of the sample i, x_i = value of the sample i, $\overline{x}$ = mean, s = standard deviation.

The 40 sampling sites with complete major ions data all have sufficient data with regard to water temperature, EC, pH, and DO. Hence, for the multivariate statistics, major ions and these four physicochemical properties were used. Principal component analysis (PCA) is a widely used tool to evaluate hydrochemical data (e.g. Fernández-Ortega et al., 2023; Spellman et al., 2024). A PCA was performed in order to identify relations between sampling groups and between hydrochemical parameters. Hierarchical cluster analysis (HCA) is a valuable tool to characterize relations of parameters and sampling sites (e.g. Merk et al., 2020; Tran et al., 2023). For this study, an HCA was performed to group the sampling sites in terms of their statistical similarities. Mean parameter values were used for each of the 40 sampling sites, clustering was done with Ward's method (Ward, 1963), and distances between the observations were calculated with the Euclidian mode. Hydrochemical similar sampling sites have a low distance on the y-axis and are grouped to a cluster, results are shown as a dendrogram.

4. Results

4.1. Spatial variations

EC indicates the total mineralization and gives a general overview of the spatial variations. EC varies strongly at spring and catchment scale (Fig. 3). Twelve outliers with EC > 1100 µS/cm within the surface streams group with minor importance for the BKS are not shown. Shale groundwater samples are generally characterized by EC < 500 µS/cm, whereas the karst water samples show a range from about 300 µS/cm (Karst DWW 3), about 400–500 µS/cm (Aa spring/stream), to about 550–1000 µS/cm (AS and MS). MS is characterized by generally higher EC values than AS. An exception is AS 2 with about 880 µS/cm ranging within the zone of MS,

representing a deeper groundwater. The Karst DWW each have individual EC ranges with overlapping zones. Karst DWW 1 shows high EC values up to 886 µS/cm, Karst DWW 2 shows intermediate EC values up to 626 µS/cm, and Karst DWW 3 shows comparatively low EC values up to 530 µS/cm. Karst GMW range between 450 and about 925 µS/cm, surface streams are characterized by a wide range from 100 to 1000 µS/cm.

Summary statistics of the major ions for the eleven sampling groups are shown in Table 1. Ca^{2+} concentrations vary between 73.6 and 112.0 mg/L for the karst springs and DWW. Highest concentrations are found at the Karst GMW group with up to 149 mg/L Ca^{2+}. Strongest spatial variations are found for Na^+ and Cl^-. For the karst groundwater, Cl^- concentrations vary by a factor of 34 between a minimum of 5 mg/L (Karst DWW 3) and a maximum of 170 mg/L (MS). Karst DWW 1 shows high Cl^- concentrations up to 101.4 mg/L, whereas Karst DWW 2 (up to 29.2 mg/L) and Karst DWW 3 (up to 15.1 mg/L) are characterized by lower concentrations. The WWIS is characterized by high K^+ (up to 25.6 mg/L), SO_4^{2-} (up to 57.5 mg/L), and NO_3^- (up to 75.5 mg/L) concentrations. The varying contents of the major ions are visualized in the Piper diagram (Fig. 4). With regard to cations, all samples are of the Ca^{2+} type, except of some WWIS samples which are of the Na^++K^+ type. With regard to anions, all samples are of the HCO_3^- type, except of some WWIS samples which are of the Cl^- type.

Compared with karst groundwater, shale groundwater samples are generally characterized by higher Mg^{2+} and SO_4^{2-} contents. The different karst groundwater sampling groups are characterized by varying Ca^{2+}, Na^+, K^+, HCO_3^-, and Cl^- contents. Aa spring/stream and Karst DWW 2 and 3 show low Na^++K^+ and Cl^- contents and low variability, while AS, MS and Karst DWW 1 are more variable with regard to these parameters.

Summary statistics of the major ions at spring scale are given in Table 2. Within the AS group, AS 3 shows lowest Cl^- concentrations of 37.2–45.2 mg/L, whereas AS 2 shows highest Cl^- concentrations > 100 mg/L. MS is characterized by overall higher Na^+ and Cl^- concentrations with a Cl^- minimum of 76.8 mg/L at MS 2. The individual spring orifices with higher Na^+ and Cl^- concentrations show slightly higher concentrations of the further major ions. Only for NO_3^- lower concentrations are found at orifices with higher Na^+ and Cl^- concentrations.

Mean proportions of the major ions are shown in Fig. 5a (catchment scale) and Fig. 5b (spring scale), circle sizes are scaled by mean TDS values. Similar samples from nearby sites were grouped together. For the WWIS group, only WWIS 1 (sampling site 39) is shown, as it is closer to the WWTP. TDS varies between a minimum of 145.6 mg/L (Shale spring 3) and a maximum of 684.1 mg/L (MS 4). Lowest TDS value of the karst groundwater is 365.7 mg/L (Karst DWW 3). With exception of WWIS 1, all sampling sites are dominated by Ca^{2+} and HCO_3^-, followed by changing proportions of Na^+ and Cl^-. For the karst groundwater, Na^+ and Cl^- proportions vary from a minimum of 4.7 % (Karst GMW 6) to a maximum of 37.4 % (MS 6). Mean Na^+ and Cl^- proportions and TDS are 22.9 % and 510.2 mg/L for ØAS, and 33.0 % and 637.3 mg/L for ØMS, respectively. Karst sampling sites located in the subcatchment show comparatively low

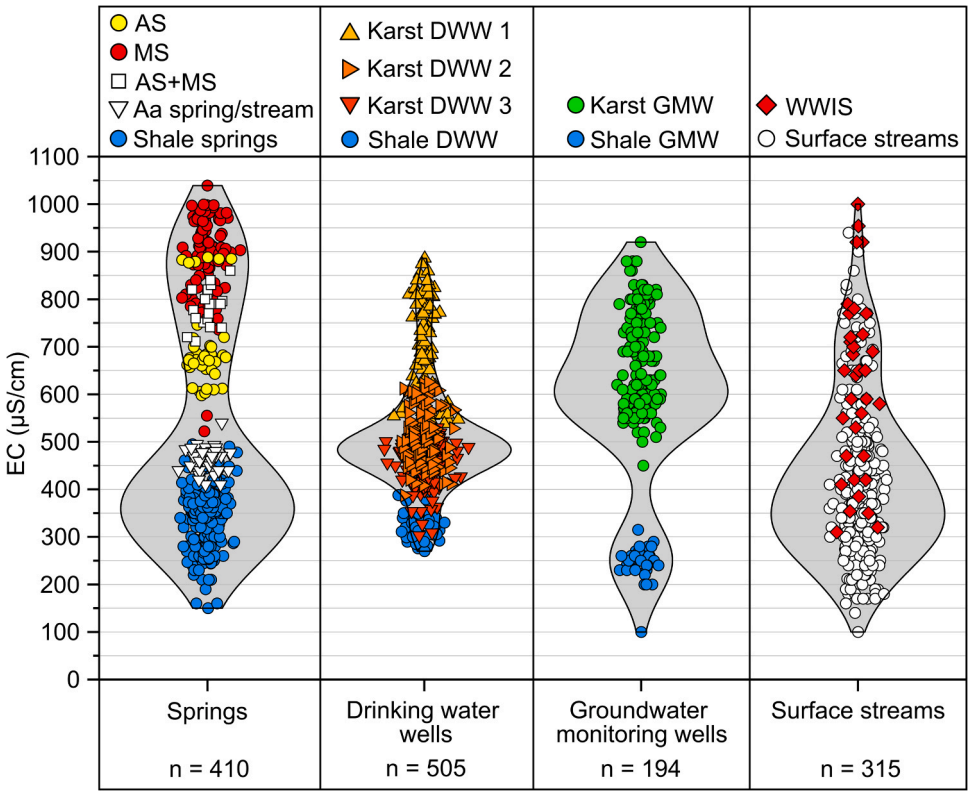

Fig. 3. EC values of the sampling groups showing spatial variations at spring and catchment scale. n = number of samples.

Table 1
Summary statistics of the major ions at catchment scale.

Sampling sites				Ca^{2+}	Mg^{2+}	Na^{+}	K^{+}	Cl^{-}	NO_3^{-}	SO_4^{2-}	HCO_3^{-}
Nr.	Group	n		(mg/L)							
1–6	AS	35	Min	83.5	8.5	19.9	1.4	37.2	20.4	18.6	240.5
			Mean	91.4	10.1	33.3	2.0	60.6	25.5	20.7	266.5
			Max	98.8	13.2	63.8	3.4	112.8	34.0	27.5	299.0
7–13	MS	47	Min	89.0	11.3	42.6	2.3	76.8	15.5	19.8	276.5
			Mean	101.6	12.2	63.1	2.8	110.9	19.6	22.8	304.4
			Max	112.0	13.1	102.0	3.3	170.0	27.1	32.1	346.6
14	AS+MS	7	Min	89.4	10.4	38.6	2.2	69.1	22.4	19.9	267.0
			Mean	94.4	10.9	45.1	2.4	80.7	23.9	21.8	272.5
			Max	99.5	11.4	55.0	2.6	101.0	30.2	26.2	280.7
15–18	Aa spring/stream	12	Min	82.2	5.2	7.4	0.8	12.9	14.3	18.0	230.2
			Mean	84.1	5.4	7.6	0.9	13.4	15.4	19.6	236.8
			Max	88.4	5.6	7.9	1.2	14.0	17.4	21.9	250.2
19	Karst DWW 1	18	Min	95.6	11.1	39.5	1.2	78.0	15.7	23.0	276.3
			Mean	100.9	12.2	45.7	1.5	87.0	18.6	25.9	299.7
			Max	107.0	13.9	54.1	2.2	101.4	21.4	30.4	314.8
20	Karst DWW 2	43	Min	86.0	6.0	3.2	0.1	7.0	10.0	14.0	258.1
			Mean	95.0	7.4	5.8	0.6	13.6	21.1	18.7	272.3
			Max	110.5	9.0	12.7	1.0	29.2	27.0	25.0	306.3
21	Karst DWW 3	24	Min	73.6	3.8	4.4	0.1	5.0	12.4	10.0	215.4
			Mean	81.0	4.8	5.6	0.6	8.8	14.7	17.2	232.9
			Max	88.6	5.4	7.9	1.0	15.1	18.0	24.0	256.9
22–30	Karst GMW	74	Min	95.8	3.0	3.1	0.4	10.0	0.4	7.8	274.6
			Mean	119.9	5.9	18.1	4.2	32.6	19.5	22.4	342.8
			Max	149.0	12.2	52.5	16.0	102.0	50.0	52.0	439.3
31–38	Shale groundwater	154	Min	21.3	2.1	3.4	0.2	3.0	6.0	4.3	50.0
			Mean	51.7	5.1	7.1	1.3	9.0	17.5	24.7	139.7
			Max	76.1	12.4	27.0	10.5	28.0	37.2	68.0	203.2
39–40	WWIS	13	Min	27.8	2.7	26.0	5.6	35.0	5.3	16.2	72.9
			Mean	63.4	5.6	63.0	12.3	95.4	29.5	32.8	176.4
			Max	92.7	10.7	269.1	25.6	416.7	75.5	57.5	286.8
41–75	Surface streams	28	Min	23.8	2.7	3.7	0.3	5.0	1.9	15.1	57.5
			Mean	55.8	5.1	15.3	2.5	24.7	12.0	31.1	148.3
			Max	105.9	10.4	73.5	13.8	128.5	41.6	93.1	323.4
		∑ 455									

TDS and Na^{+} and Cl^{-} proportions. Within the Karst GMW group, only Karst GMW 4 (12.6 %) and Karst GMW 5 (21.0 %) show Na^{+} and Cl^{-} proportions > 10 %. Notable K^{+} proportions are found at WWIS 1, Karst GMW 5 and Surface stream 7.

Cl^{-} concentration zones of AS as found in August 1943 are given in Koch and Vogel (1992), the zones are shown in Fig. 6a. Overall, results from sampling sites 1–4 confirm the delineated zones (compare with Table 2). Results from sampling sites 7–13 allow for the first time to delineate such zones for MS in the same way (Fig. 6b). Due to the higher concentrations at MS, two zones are delineated ranging from 77 to 90 mg/L, and > 88 mg/L, respectively.

Concentrations and relations of Ca^{2+}, Mg^{2+}, and HCO_3^{-} are shown in Fig. 7. Karst and shale groundwater can be distinguished by Ca^{2+} concentrations, as they have no overlap zone (Fig. 7a). Generally, MS > AS > Aa spring/stream, and Karst DWW 1 > Karst DWW 2 > Karst DWW 3. Significantly higher Ca^{2+} concentrations are found for the Karst GMW shown in green. Karst groundwater samples are distributed along the calcite dissolution ratio of 1:1, with Karst GMW having a more diffuse distribution (Fig. 7b). Mg^{2+} concentrations vary at spring and catchment scale with a similar pattern as Ca^{2+}. Karst DWW show distinct concentrations without overlap zones (Fig. 7c). The scatterplot of Ca^{2+} and Mg^{2+} reveals distinct clusters for the karst groundwater sampling groups, whereas surface streams are more diffusely distributed (Fig. 7d). Karst DWW 3 and Aa spring/stream represent the subcatchment and form a cluster. Ca^{2+}/Mg^{2+} ratios for each of the 40 sampling sites with complete major ions data are depicted in Fig. S7 in the electronic supplementary material.

4.2. Origin of sodium and chloride

Concentrations and relations of Na^{+}, Cl^{-}, Mg^{2+}, and K^{+} are shown in Fig. 8. One outlier from the WWIS group with a Cl^{-} concentration of 416.7 mg/L is not shown, but included in Table 1. The Karst GMW group is further distinguished for Fig. 8 to emphasize the correlation of Karst GMW 5 with WWIS (see Fig. legend). Chloride concentration patterns of the sampling groups are similar to Ca^{2+} and Mg^{2+} (Fig. 8a). Karst springs, DWW, and most GMW are well distributed along the seawater evaporation Na^{+}/Cl^{-} ratio of 0.86. On the contrary, WWIS and Karst GMW 5 are distributed along the halite dissolution ratio of 1:1 (Fig. 8b). Higher Na^{+} and Cl^{-} concentrations are associated with slightly higher concentrations of Mg^{2+} and K^{+} (Fig. 8c,d). Karst groundwater samples show a good fit with the seawater evaporation ratios for these parameters, too, whereas Karst GMW 5 forms a cluster with the WWIS group.

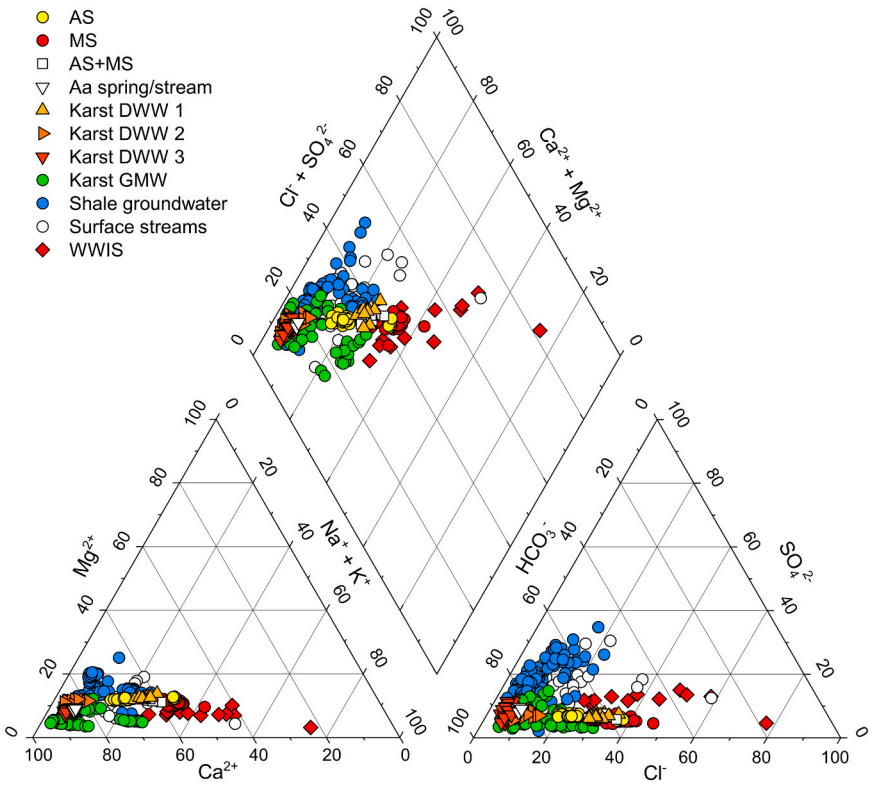

Fig. 4. Piper diagram showing hydrochemical variations of the eleven sampling groups.

4.3. Correlations of chloride with other parameters

Table 3 lists the correlations of chloride with other parameters as found with the Spearman rank correlation test for the 2020–2021 data. Results are sorted from stronger to weaker correlations. For the karst groundwater, chloride correlates positively with EC, water temperature, and all further major ions, with the exception of NO_3^-. Positive correlations are found with the trace elements Li, Rb, Sr, Cs, U, Ba, and Ti, too. Negative correlations are found with NO_3^-, DO, and Cr. For the surface streams, positive correlations were found with Na^+, K^+, NO_3^-, DOC, EC, Gd, TOC, SO_4^{2-}, and some trace elements.

Scatterplots of Cl^- with selected correlating parameters are shown in Fig. 9 and in Fig. S8 in the electronic supplementary material. With regard to the karst springs AS and MS, the positive correlation of Cl^- with the trace elements lithium, uranium, rubidium, strontium, and cesium is almost a linear relation (Fig. 9a-e). Karst DWW 1 has similar Cl^- concentrations as sampling site AS+MS, representing the mean of AS and MS. It could be expected that the trace element concentrations of Karst DWW 1 are thus similar to AS+MS. In contrast, the trace element concentrations of Karst DWW 1 are always lower, and differ from the linear relation of the karst springs. Interestingly, the major ions concentrations of Karst DWW 1 and AS+MS are similar (see Figs. 7 and 8). These findings suggest differences between the sampling site types, with different waters reaching the karst springs and the DWW. It is also interesting to note that compared to MS, AS 2 exhibits slightly higher concentrations for most trace elements. Maximum trace element concentrations in the karst groundwater are 54.4 µg/L for Li, 1.36 µg/L for U, 17.2 µg/L for Rb, 387.3 µg/L for Sr, 6.3 µg/L for Cs, 76.2 µg/L for Ba, and 0.7 µg/L for Ti. The negative correlation of Cl^- with NO_3^- is shown in Fig. 9 g. While AS is characterized by NO_3^- concentrations of 20.4–34.0 mg/L, MS has overall lower concentrations of 15.5–27.1 mg/L. Higher Cl^- concentrations also correlate with lower DO saturations (Fig. 9 h).

4.4. Seasonal variations

Discharge of AS+MS with precipitation and groundwater levels are depicted in Fig. 10 for the time period of the six sampling campaigns 2020–2021. Elevation levels of the Aa karst spring draining the subcatchment, and of AS and MS are shown, too. The sampling campaigns cover nearly all typical hydrological states of an annual cycle of the BKS: Declining discharge and water levels in September 2020, lowest levels in November and December 2020, an increase in January 2021, and high values in March 2021. Only the typical maximum discharge of around 1.2 m^3/s in spring time was not reached in 2021. Compared with the main catchment, groundwater levels in the subcatchment are higher and show less pronounced variations over an annual cycle.

Cl^- and NO_3^- concentrations are shown over the course of the six sampling campaigns in Fig. 11. The concentrations remain fairly stable throughout the year in the karst groundwater, with no clear seasonal changes. Even the high Cl^- concentration of 416.7 mg/L at

Table 2
Summary statistics of the major ions at spring scale.

Sampling sites				Ca^{2+}	Mg^{2+}	Na^{+}	K^{+}	Cl^{-}	NO_3^{-}	SO_4^{2-}	HCO_3^{-}
Nr.	Name	n		(mg/L)							
1	AS 1	6	Min	91.0	9.6	27.6	1.7	50.2	23.9	19.7	269.6
			Mean	95.1	10.4	31.4	2.0	58.3	26.8	20.9	275.5
			Max	98.8	10.9	38.5	2.3	71.6	30.1	23.7	286.8
2	AS 2	6	Min	91.8	12.4	59.6	1.6	104.0	20.4	21.2	280.3
			Mean	93.8	12.8	61.5	2.9	107.3	21.4	22.5	288.4
			Max	96.9	13.2	63.8	3.3	112.8	24.0	27.5	299.0
3	AS 3	6	Min	83.5	8.5	19.9	1.4	37.2	24.2	18.6	240.5
			Mean	87.4	8.6	21.4	1.9	40.5	25.4	20.0	247.7
			Max	89.2	8.9	22.6	3.4	45.2	27.3	21.7	265.4
4	AS 4	5	Min	92.3	9.3	23.0	1.5	41.8	29.5	19.0	264.2
			Mean	94.1	9.7	26.3	1.7	48.6	30.8	19.8	269.2
			Max	97.1	10.3	28.2	1.8	51.9	34.0	20.1	277.2
5	AS 5	6	Min	87.6	9.2	26.1	1.7	49.7	24.5	19.2	250.9
			Mean	89.2	9.5	27.9	1.8	51.5	25.0	20.3	261.3
			Max	91.5	9.8	29.0	1.9	53.9	26.3	23.4	269.6
6	AS 6	6	Min	86.5	9.3	26.4	1.7	47.8	23.7	18.9	246.2
			Mean	89.3	9.7	30.3	2.0	55.2	24.4	20.5	257.5
			Max	93.4	10.2	34.1	2.1	64.3	26.2	23.6	268.5
7	MS 1	5	Min	97.6	11.7	43.5	2.3	78.3	19.6	19.8	290.7
			Mean	98.6	12.1	46.4	2.5	84.0	21.6	21.3	293.0
			Max	100.5	12.5	49.5	2.6	89.8	24.0	25.6	296.4
8	MS 2	6	Min	95.2	11.5	42.6	2.4	76.8	20.4	19.9	284.9
			Mean	97.1	11.9	43.4	2.5	79.1	21.5	21.1	290.4
			Max	99.6	12.3	46.4	2.7	82.2	25.7	25.9	299.2
9	MS 3	6	Min	95.2	11.7	49.3	2.7	87.6	18.2	20.6	280.1
			Mean	97.2	12.2	54.4	2.8	96.0	20.1	22.2	293.0
			Max	101.2	12.8	65.1	2.9	111.5	23.3	28.3	305.1
10	MS 4	13	Min	98.6	11.3	66.8	2.7	110.0	17.4	20.0	305.9
			Mean	106.6	11.8	71.1	2.9	124.3	19.7	23.6	324.1
			Max	112.0	12.6	75.0	3.1	136.5	27.1	30.0	346.6
11	MS 5	6	Min	97.3	12.3	61.2	2.8	108.6	17.8	21.6	288.7
			Mean	100.9	12.8	64.4	2.9	114.2	19.6	23.9	299.8
			Max	104.1	13.1	67.7	3.1	120.5	23.8	32.1	305.9
12	MS 6	5	Min	89.0	11.5	63.6	2.6	109.5	16.0	19.9	276.5
			Mean	99.0	12.4	75.9	3.0	128.7	17.0	21.7	296.9
			Max	104.1	13.1	102.0	3.3	170.0	18.1	22.9	305.9
13	MS 7	6	Min	102.2	12.2	73.2	3.0	127.8	15.5	22.9	295.5
			Mean	104.8	12.5	75.8	3.2	133.0	17.3	24.6	307.5
			Max	109.4	13.0	78.0	3.3	141.8	22.0	30.5	312.5
		∑ 82									

WWIS 1 in January 2021 does not affect the karst groundwater (Fig. 11a). In contrast, compared with the karst groundwater, Surface stream 16 starts with significantly lower NO_3^- concentrations in September 2020, increases to a maximum of 40.3 mg/L in January 2021, and eventually decreases again to lower concentrations in spring 2021. WWIS 1 shows highest NO_3^- concentrations for most parts of the year (Fig. 11b).

AS 2 is a spring orifice that emerges directly from a small rock crevice just above the AS pond, representing the deeper karst groundwater with higher Na^+ and Cl^- concentrations. At a constant value of 11.1 °C, water temperature of AS 2 did not vary at all over the six sampling campaigns. Other parameters as EC (877–888 μS/cm) and DO (57.3–63.1 %) were quite constant, too. In contrast, the discharge of this orifice (observed by visual inspection) varied strongly with lowest discharge in autumn and highest discharge in spring. AS 2 is an example that varying discharge does not necessarily lead to varying hydrochemistry. The higher discharge in spring is explained by a stronger hydrostatic pressure in times of groundwater recharge, when the BKS is filled up with younger groundwater in surface-near sections of the aquifer.

4.5. Gadolinium

Normalized mean REE concentrations of the sampling groups are shown in Fig. 12a. A strong positive Gd anomaly is found for WWIS 1. Compared with karst groundwater, the surface streams exhibit overall higher REE concentrations. Gd concentrations of WWIS 1 are high throughout an annual cycle, no direct impact on the karst groundwater was found (Fig. 12b). Absolute Gd concentrations for WWIS 1 range from 52.3 to 1538.1 ng/L, with a mean of 474.5 ng/L. For the karst groundwater, absolute concentrations range from 0.9 to 18.6 ng/L, with a mean of 2.1 ng/L.

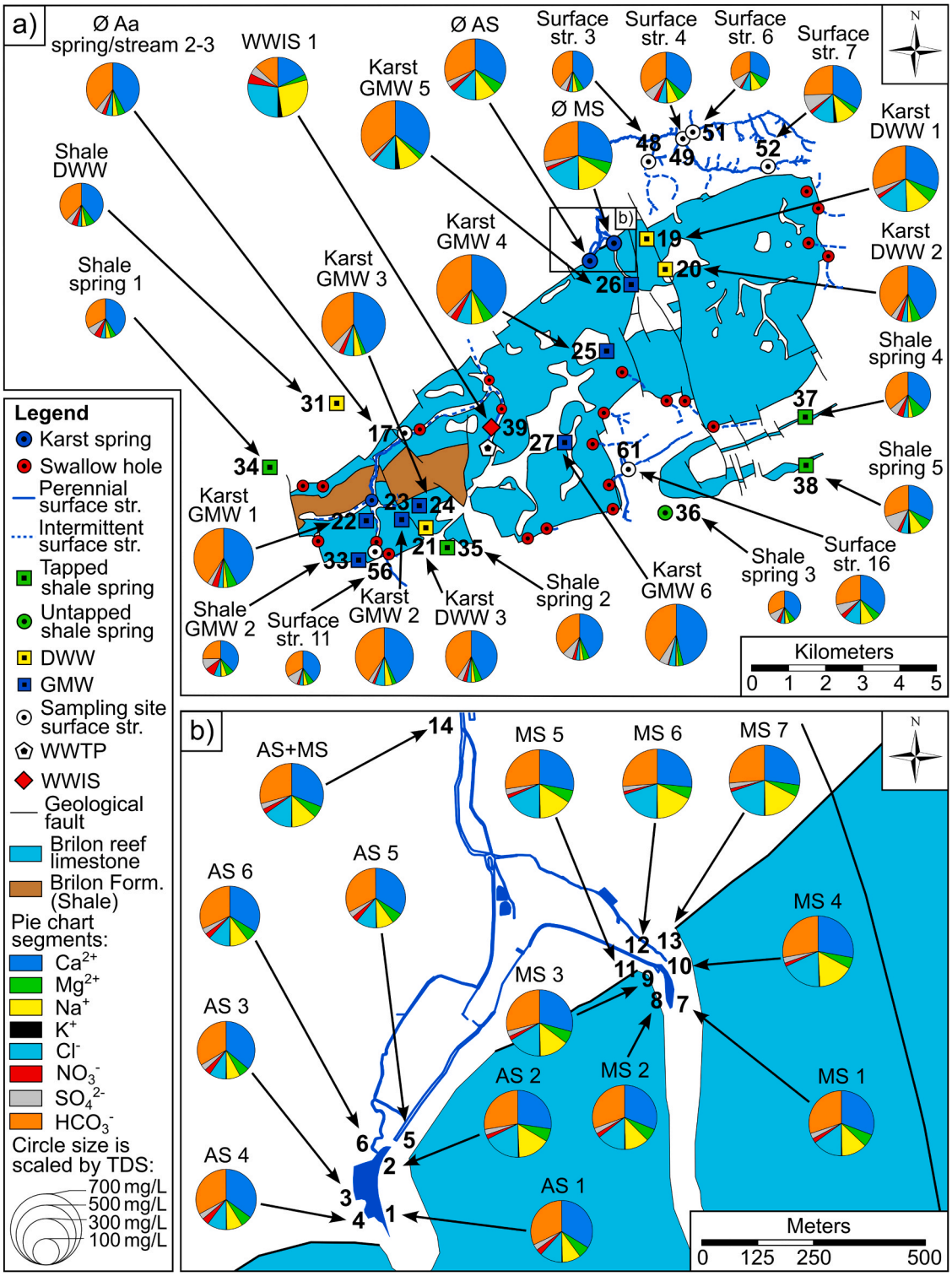

Fig. 5. Hydrochemical map of the Brilon karst system with pie charts showing mean proportions of major ions, circle sizes are scaled by TDS. Base map: Geological Service NRW (2024). a) Catchment scale. b) Spring scale.

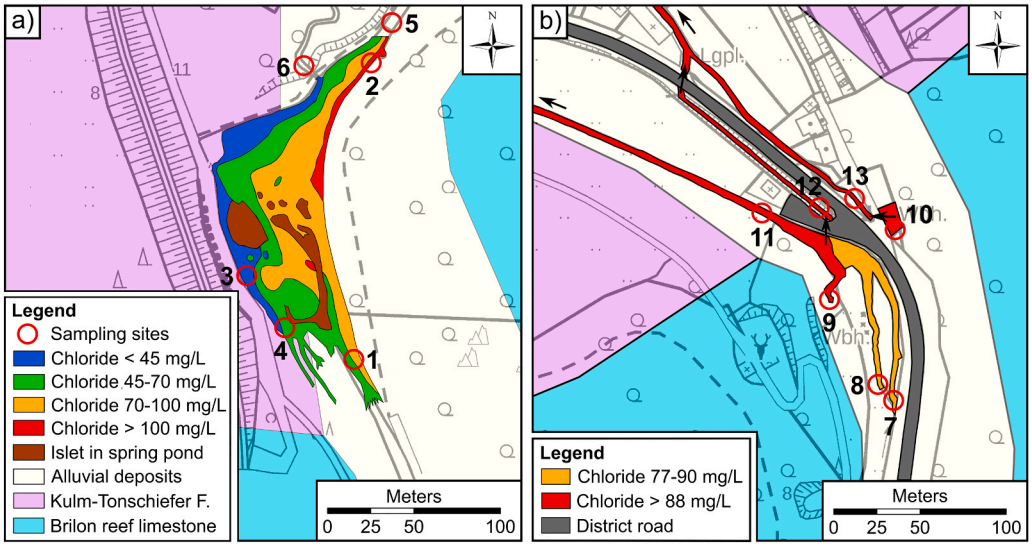

Fig. 6. Chloride concentration zones at spring scale. Base maps: Geological Service NRW (2024), Bezirksregierung Köln (2024b). a) AS, as found in August 1943, modified after Koch and Vogel (1992). b) MS, as found during the six sampling campaigns 2020–2021.

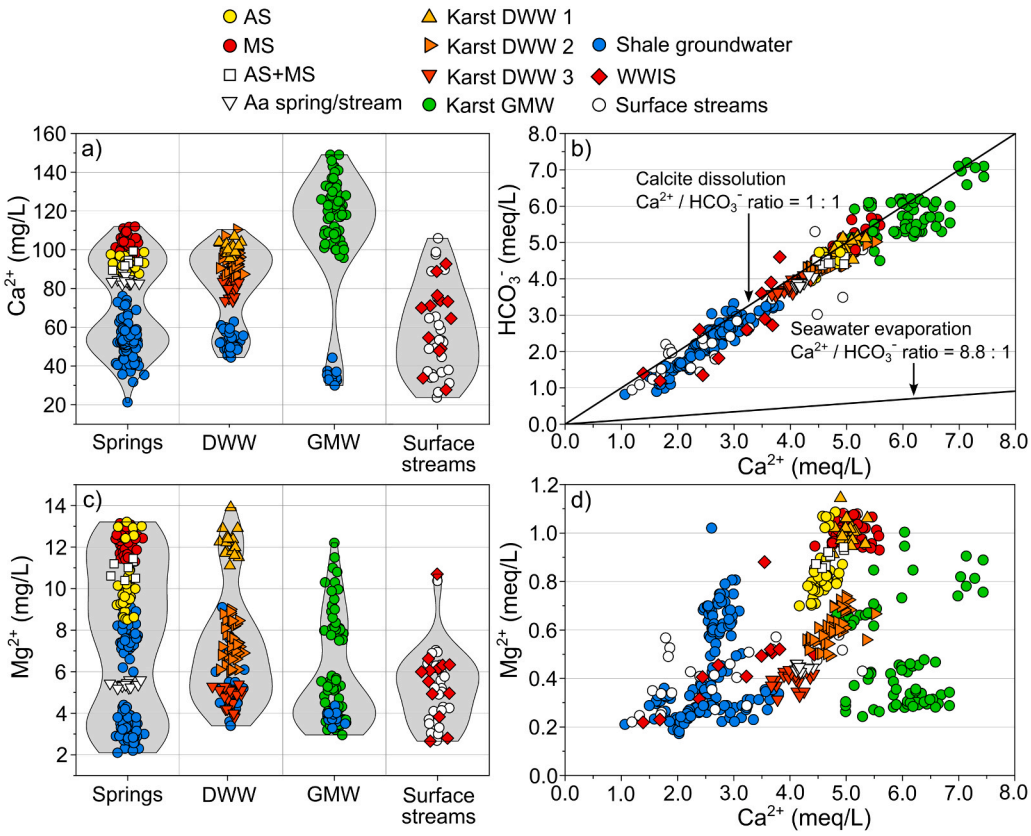

Fig. 7. Variations and correlations of Ca^{2+}, HCO_3^-, and Mg^{2+}. a) Violin plot of Ca^{2+}. b) Scatterplot of Ca^{2+} and HCO_3^-. c) Violin plot of Mg^{2+}. d) Scatterplot of Ca^{2+} and Mg^{2+}.

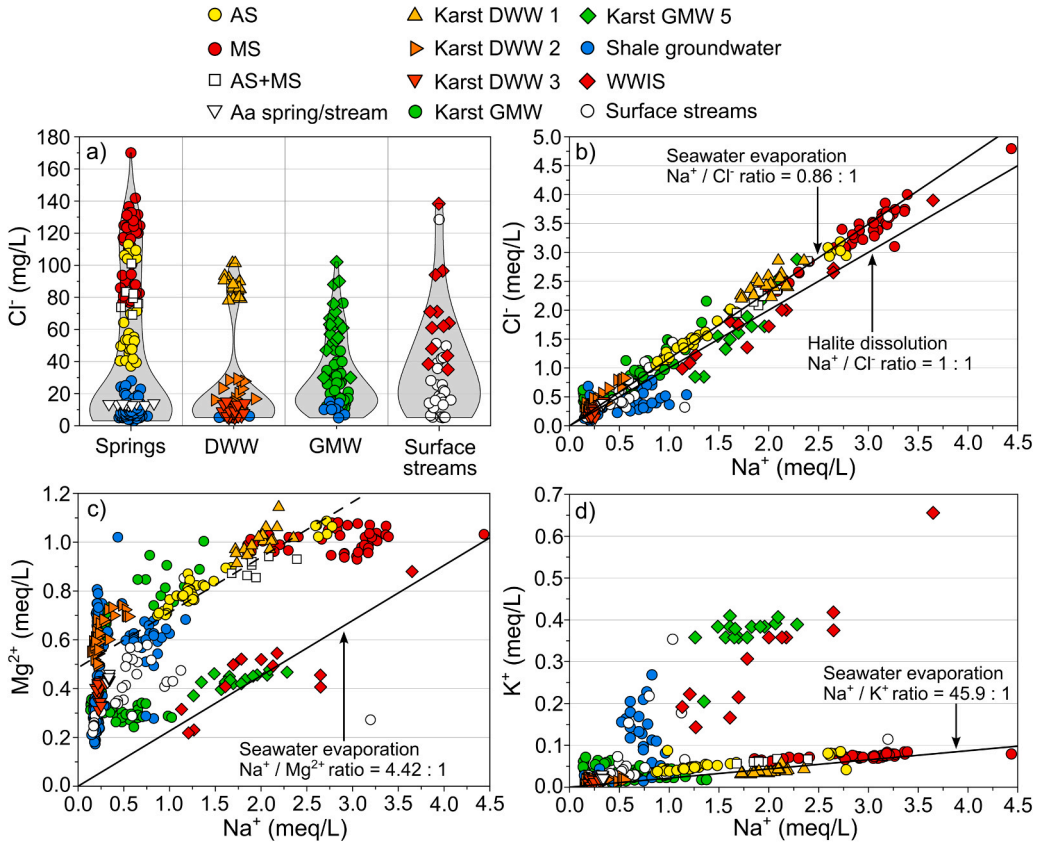

Fig. 8. Variations and correlations of Na^+, Cl^-, Mg^{2+}, and K^+. a) Violin plot of Cl^-. b) Scatterplot of Na^+ and Cl^-. c) Scatterplot of Na^+ and Mg^{2+}. d) Scatterplot of Na^+ and K^+.

Table 3
Spearman rank correlations of chloride with further parameters for the 2020–2021 data.

Karst groundwater		**Surface streams/WWIS**	
	Cl^-		Cl^-
Na^+	0.99	Na^+	0.89
EC	0.99	K^+	0.76
Mg^{2+}	0.87	Co	0.72
Li	0.87	Cu	0.71
HCO_3	0.86	Cs	0.71
Rb	0.86	Rb	0.64
Sr	0.85	Mn	0.63
Cs	0.84	NO_3	0.58
K^+	0.83	Ni	0.58
U	0.79	DOC	0.56
Ba	0.79	EC	0.55
Ca^{2+}	0.76	Gd	0.55
SO_4^{2-}	0.74	TOC	0.53
Ti	0.66	Ga	0.53
Water Temp.	0.58	V	0.50
NO_3	-0.49	SO_4^{2-}	0.50
DO	-0.46	Li	0.49
Cr	-0.46	DO	-0.46

4.6. Long-term trends

Long-term Cl^- concentration trends of the four sampling sites used for the drinking water supply are shown in Fig. 13. MS 4 and Karst DWW 1 exhibit strong and significantly increasing trends. MS 4 was already characterized by high concentrations around 100 mg/L in the 1980s. Today, concentrations exceed 120 mg/L. On the other hand, Karst DWW 1 started with low concentrations

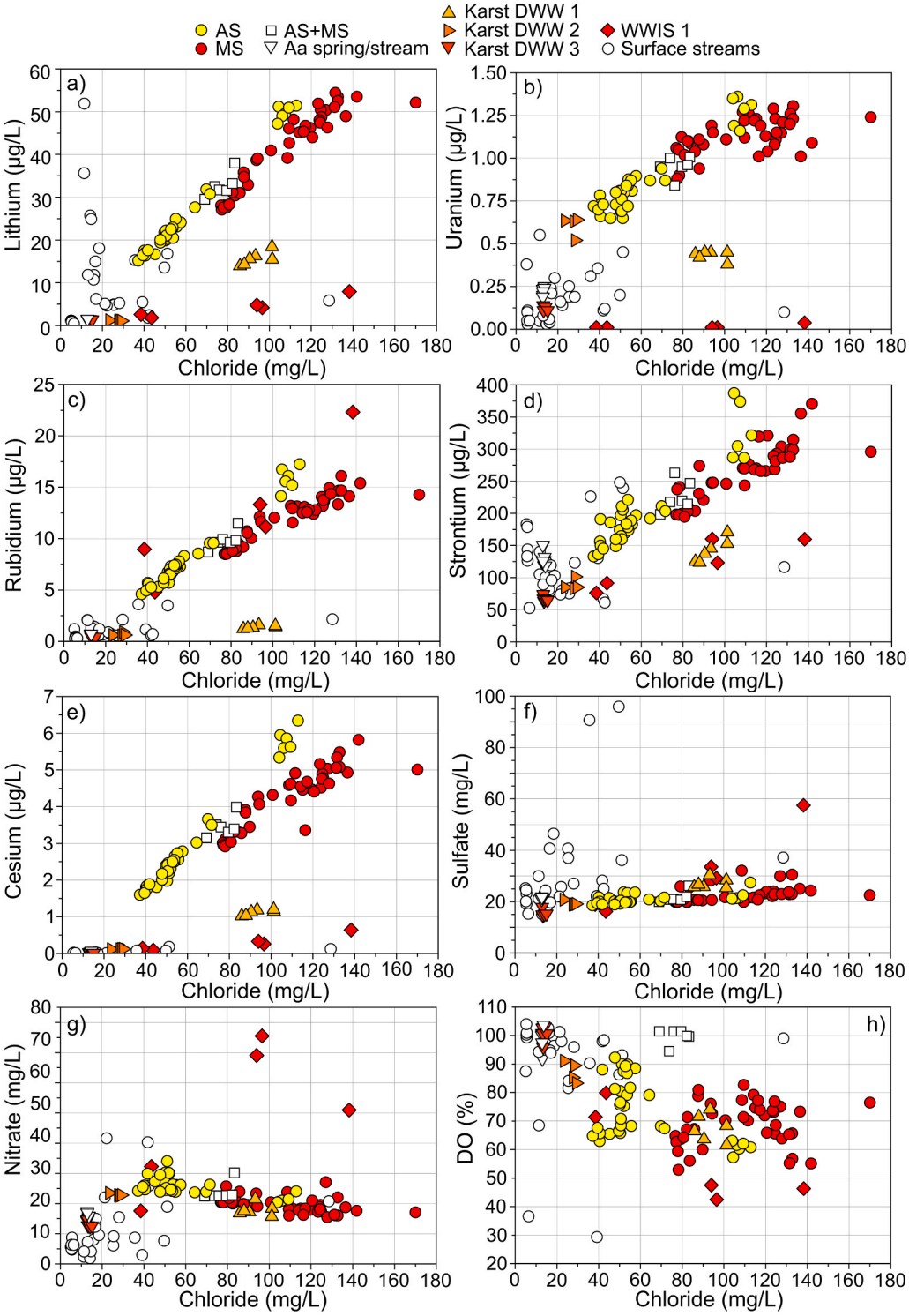

Fig. 9. Correlations of chloride with a) lithium, b) uranium, c) rubidium, d) strontium, e) cesium, f) sulfate, g) nitrate, and h) DO.

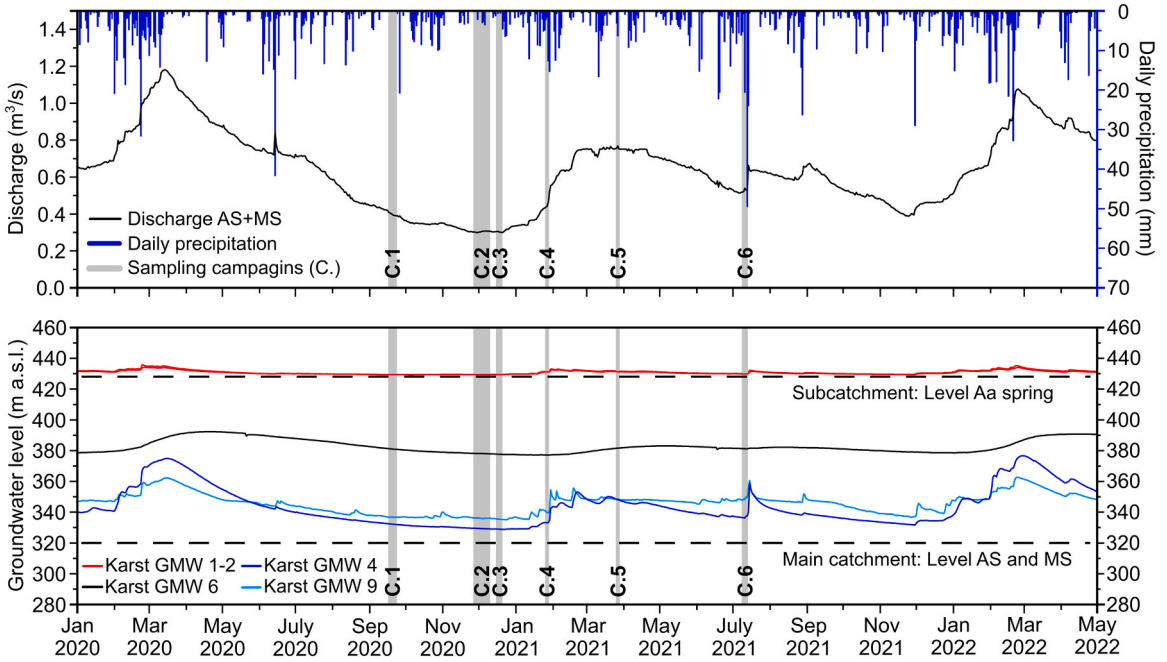

Fig. 10. Seasonal variations of discharge and precipitation (upper), and groundwater levels (lower) during the six sampling campaigns 2020–2021.

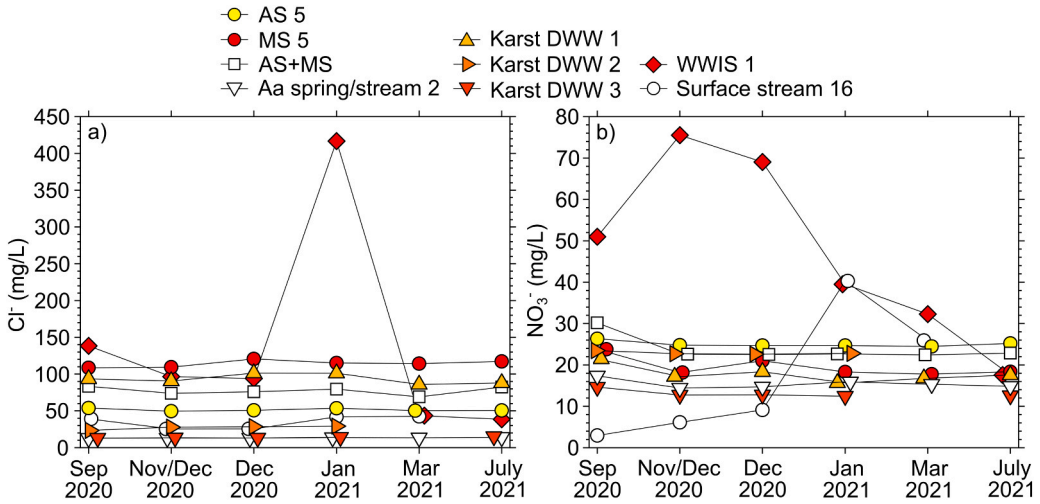

Fig. 11. Seasonal variations of a) chloride concentrations, and b) nitrate concentrations during the six sampling campaigns 2020–2021.

around 30 mg/L in the 1980s and is around 90 mg/L today. For Karst DWW 2 an overall slow but significantly increasing trend is found, too. However, elevated concentrations of up to 32 mg/L were only observed between 2012 and 2022, and today's concentrations of around 14 mg/L are only slightly higher compared with those from the 1980s. No significant trend is found for Karst DWW 3, overall concentrations are low and similar to Karst DWW 2. For Na^+, Ca^{2+}, and Mg^{2+}, all four sampling sites show significantly increasing trends. Long-term NO_3 concentrations are shown in Fig. S9 in the electronic supplementary material, they were initially characterized by a significant increase, too. In contrast, MS 4 shows stable concentrations of around 19 mg/L since 1995, and the Karst DWW are characterized by significantly decreasing concentrations since 2008 (Karst DWW 1), 2013 (Karst DWW 2), and 1987 (Karst DWW 3).

4.7. Multivariate statistics

Correlations between sampling groups and hydrochemical parameters determined with the PCA are shown in Fig. 14a. Two outliers from the WWIS group are not shown. PC1 explains 41.22 % of the observations, while PC2 explains 13.29 % of the observations. The

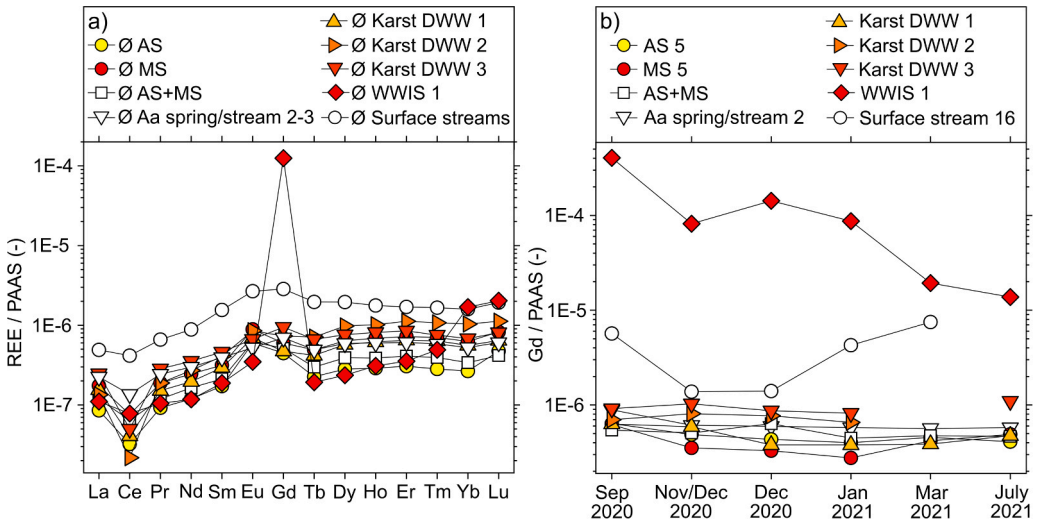

Fig. 12. Normalized REE concentrations. a) Mean values of the sampling groups. b) Gadolinium concentrations during the six sampling campaigns 2020–2021.

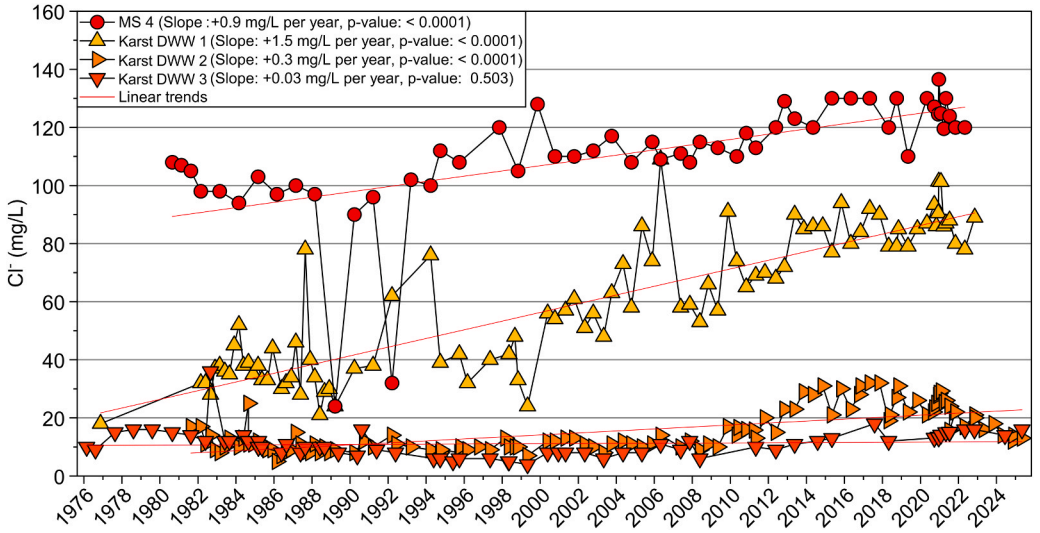

Fig. 13. Long-term data of chloride for sampling sites MS 4 and Karst DWW 1–3 including linear trends.

rather low total percentage (54.51 %) is an expression of the hydrochemical complexity of the BKS. A strong correlation is found for Ca^{2+} and HCO_3^-. Due to the high Ca^{2+} and HCO_3^- concentrations of some Karst GMW, they are associated with these parameters. Na^+ and Cl^- are strongly related. Together with EC, Mg^{2+} and, to a lesser extent, water temperature they represent the deeper groundwater and are related with MS, Karst DWW 1 and AS 2. NO_3^- does not show a clear correlation with other parameters, but is placed with AS and the Karst GMW. K^+ and SO_4^{2-} are correlated with WWIS samples. DO and pH are the only parameters on the negative axis of PC1 and are therefore more correlated with shale groundwater and surface streams. Due to low Na^+ and Cl^- concentrations, Karst DWW 3 and Aa spring/stream representing the subcatchment are associated with shale groundwater samples.

HCA results are shown in Fig. 14b. Most shale groundwater and surface streams sampling sites are grouped together in cluster 2. Exceptions are Shale spring 5 and Surface stream 7, which exhibit high K^+ concentrations. Therefore, together with WWIS 1–2 and Karst GMW 5, they form a subgroup within cluster 1. Due to their low Na^+, Cl^-, Ca^{2+}, and HCO_3^- concentrations, Karst DWW 3 and Aa spring/stream 2–3 are grouped with shale and surface stream sampling sites in cluster 2. This relationship is also evident from the PCA results (Fig. 14a). Subgroups of cluster 1 result from the varying Na^+ and Cl^- proportions, as well as differences in the Ca^{2+} and HCO_3^- proportions. Karst springs with intermediate Na^+ and Cl^- concentrations form a subgroup including all AS springs and AS+MS except of AS 2, which is grouped with the MS subgroup due to high Na^+ and Cl^- concentrations. Karst DWW 1 is included in the MS subgroup, whereas Karst DWW 2 is grouped along with Karst GMW (low Na^+ and Cl^- concentrations).

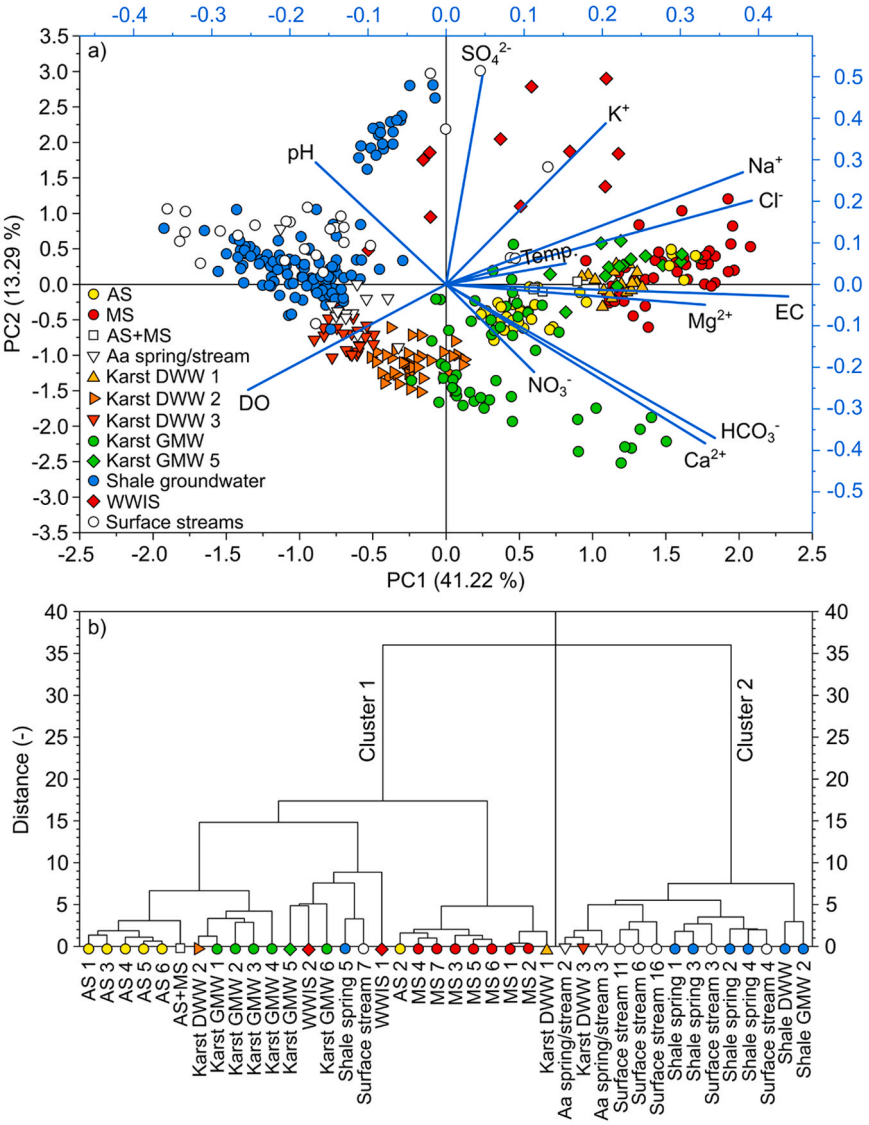

Fig. 14. Multivariate statistics. a) Principal component analysis of all individual samples. b) Hierarchical cluster analysis of mean values for each sampling site.

5. Discussion

The results of this study enable the first comprehensive hydrogeological and hydrochemical conceptual model of the Brilon karst system (BKS) and its karst springs, and provide new insights into the understanding of deep karst systems in general. The BKS is generally controlled by a duality between influences coming from the surface and from deeper groundwater rising to the surface. In contrast to typical shallow karst systems, impacts from the surface are rather low and the BKS is mainly controlled by deeper groundwater. EC, Ca^{2+} and Cl^- concentrations of the BKS exceed typical values for pure carbonate aquifers. Pulido-Bosch (2021) states typical values from 50 to 100 mg/L for Ca^{2+}, < 20 mg/L for Cl^-, and a range from 300 to 700 µS/cm for EC. Kilchmann et al. (2004) found EC values from 147 to 609 µS/cm for carbonate aquifers. EC values > 600 µS/cm often derive from sulfates, chlorides, or contamination with nitrate (Ford and Williams, 2007). The BKS is affected by groundwater that was in contact with other rock types.

5.1. Origin of sodium and chloride

Ca^{2+} and HCO_3^- stem from calcite dissolution (Fig. 7b) and thus originate directly from the Brilon reef limestone. With exception of Karst GMW 5, all karst groundwater samples are well distributed along the seawater evaporation ratios of Na^+/Cl^-, Na^+/K^+, and, to a lesser extent, Na^+/Mg^{2+} (Fig. 8b-d). Thus, these parameters originate from the dissolution of evaporites. It is assumed that water which

was in contact with evaporites enters the BKS via deep faults. A possible provenience area is the Münsterland Cretaceous Basin north of the BKS, where highly mineralized brines are well-known (Grobe and Machel, 2002). Another possible provenience area is the Rhenish Slate Mountains south of the BKS, where waters with high mineralization are known, too (Heuser, 2017). The salinity could also stem from deeper parts of the BKS itself. In large karst aquifers, where evaporites were deposited along with carbonates, original seawater can be preserved in deeper sections of the aquifer, as described from the Floridan aquifer system (Williams and Kuniansky, 2016).

A Na^+ and Cl^- source coming from the surface is the application of road salt (Panno et al., 2006), which consists of the mineral halite. WWIS and Karst GMW 5 are distributed along the halite dissolution ratio (Fig. 8b) and are therefore associated with road salt, which is washed into the sewerage system in winter. Hence, two origins of Cl^- can be distinguished in the BKS via the Na^+/Cl^- ratio: Cl^- in the deeper groundwater originating from the dissolution of evaporites, and Cl^- related to road salt from the surface sinking into the BKS via swallow holes. High K^+ concentrations are typically related with waste waters (Hamdan et al., 2020). The high K^+ concentrations and the correlation with WWIS (Fig. 8d) indicate a contamination with waste water at Karst GMW 5.

5.2. Correlations of chloride with other parameters

Typical trace elements associated with karst water that was in contact with evaporites are Sr and Ba originating from the dissolution of celestite and barite, as well as Li and Rb originating from brine inclusions (Kilchmann et al., 2004; Hunkeler and Mudry, 2007). This corroborates with the correlations of Cl^- with trace elements as found with the Spearman rank correlation test (Section 4.3). Sr concentrations are often particularly high (Hunkeler and Mudry, 2007), which is confirmed by the high Sr concentrations of up to 387.3 µg/L found in the BKS (Fig. 9d). A contradiction are the rather low sulfate concentrations with a mean of 22.8 mg/L at MS (Table 1, Fig. 9 f). Waters related to evaporites are usually dominated by sulfate stemming from the dissolution of gypsum (Gong et al., 2025). Contrary, the BKS groundwater is dominated by Na^+ and Cl^-. This means that little or no gypsum layers are involved in the water-rock interactions of the deeper karst groundwater in the BKS area.

5.3. Seasonal variations

The AS+MS hydrograph differs from typical karst systems (Fig. 10). Karst spring hydrographs often show fast and strong reactions to precipitation events, with discharge varying through several orders of magnitude in very short time periods (Goldscheider et al., 2007). In contrast, the AS+MS discharge and groundwater levels show a rather smooth and balanced behavior over an annual cycle with variations at seasonal scale. There are no direct and rapid reactions to precipitation events, except for heavy rainfall. The balanced hydrograph and groundwater levels indicate that the BKS is not highly karstified, with no large conduits connecting the surface with AS and MS. This is also confirmed by the flat chemographs of Cl^- and NO_3^- (Fig. 11). Highly karstified aquifers with a pronounced conduit porosity show rather fluctuating chemographs (Hunkeler and Mudry, 2007).

NO_3^- concentrations of surface streams typically vary over an annual cycle with highest values in winter, when fertilizers are washed from the land surface into the streams (Mahler et al., 2008; Strebel et al., 1989). At the BKS this pattern was found for Surface stream 16 (Fig. 11b). Karst groundwater samples show higher NO_3^- concentrations for most of the year. Only in winter, Surface stream 16 has higher NO_3^- concentrations compared to the karst groundwater. The findings show that NO_3^- is infiltrating into the BKS as a contaminant. The concentrations of up to 34.0 mg/L (AS) and 27.1 mg/L (MS) are elevated compared with uncontaminated karst systems. However, as the BKS is predominantly controlled by deeper groundwater, impacts from the surface are attenuated.

In pristine, near-surface karst groundwater, DO saturation is often around 100 % (Stevanović et al., 2024). Large aquifers have almost constant water temperatures throughout the year, whereas shallow waters in the epikarst zone exhibit highly variable water temperatures over time (Pulido-Bosch, 2021). The mean annual air temperature of the Brilon area is 8.9 °C for the period 2005–2025 (German Meteorological Service, 2026). Water temperatures of the deeper groundwater are higher and show no variations throughout an annual cycle at some sampling sites (Section 4.4). The constant water temperature of 11.1 °C and the low DO saturations between 57.3 % and 63.1 % at AS 2 prove that the deeper groundwater is mostly separated and uncoupled from the surface-near recharge zones.

5.4. Long-term trends and implications for the drinking water supply

Koch (1998) states mean residence times of 30–50 years for the deeper karst groundwater. Consequently, hydrochemical variations are assumed to take place at a long-term scale, rather than on a seasonal scale. Accordingly, in extreme cases an infiltrating contaminant will reach the karst springs only after 50 years. This would mean that the signals from 1975 will not reach AS and MS as well as the Karst DWW until 2025. It must also be emphasized, that the deep and slow groundwater flow paths lead to a slow but steady accumulation of contaminants within the BKS. The accumulation cannot be reversed. Cl^- concentration zones at AS as found in August 1943 are overall still valid to date (Section 4.1, Fig. 6a). The significantly increasing long-term concentrations of Cl^- (Fig. 13) are related to a growing influence of the deeper groundwater. Trace elements correlated with Cl^- (Fig. 9) are therefore expected to show increasing trends, too. As the trace element concentrations are far below of common guideline values for drinking water, this won't lead to implications for the drinking water supply. The guideline value for U is 30 µg/L (European Union, 2020; WHO, 2022), whereas the maximum concentration in the BKS is 1.36 µg/L. Guideline values for Cl^- (250 mg/L) and NO_3^- (50 mg/L) are also complied with. The significantly decreasing long-term NO_3^- concentrations are in line with the negative correlation with Cl^- found with the Spearman rank correlation test. As the deeper karst groundwater is depleted in NO_3^-, increasing Cl^- trends lead to decreasing NO_3^- concentrations. The characteristics of the deeper groundwater are favorable for the drinking water supply. Decreasing NO_3^- concentrations, as well as the low influence of contaminants coming from the surface, favor the use of the deeper groundwater for the drinking water supply.

Nevertheless, monitoring of critical parameters should be continued. Especially NO_3^- concentrations are close to the guideline value, and unlike today, showed increasing trends until 2008 (Karst DWW 1), and 2013 (Karst DWW 2). Shifting influences from the surface and from the deeper groundwater could be identified by continued monitoring and help to further improve the understanding of the BKS.

5.5. Limitations and future research

At the temporal scale, this study is limited to seasonal and long-term variations. However, typical karst aquifers are strongly influenced from the surface and react rapidly to precipitation events (White, 1999). To capture the high temporal variability of hydrochemical processes, event-based high-resolution monitoring and continuous sampling is widely used in karst research (Huebsch et al., 2014; Goldscheider, 2015). High-resolution monitoring proved valuable to achieve deeper insights into karst aquifers (e.g. Frank et al., 2022; Mueller et al., 2025). In order to determine possible fast surface-subsurface interactions, future research at BKS should also include a high-resolution monitoring of hydrological events (strong precipitation) at both swallow holes and karst groundwater.

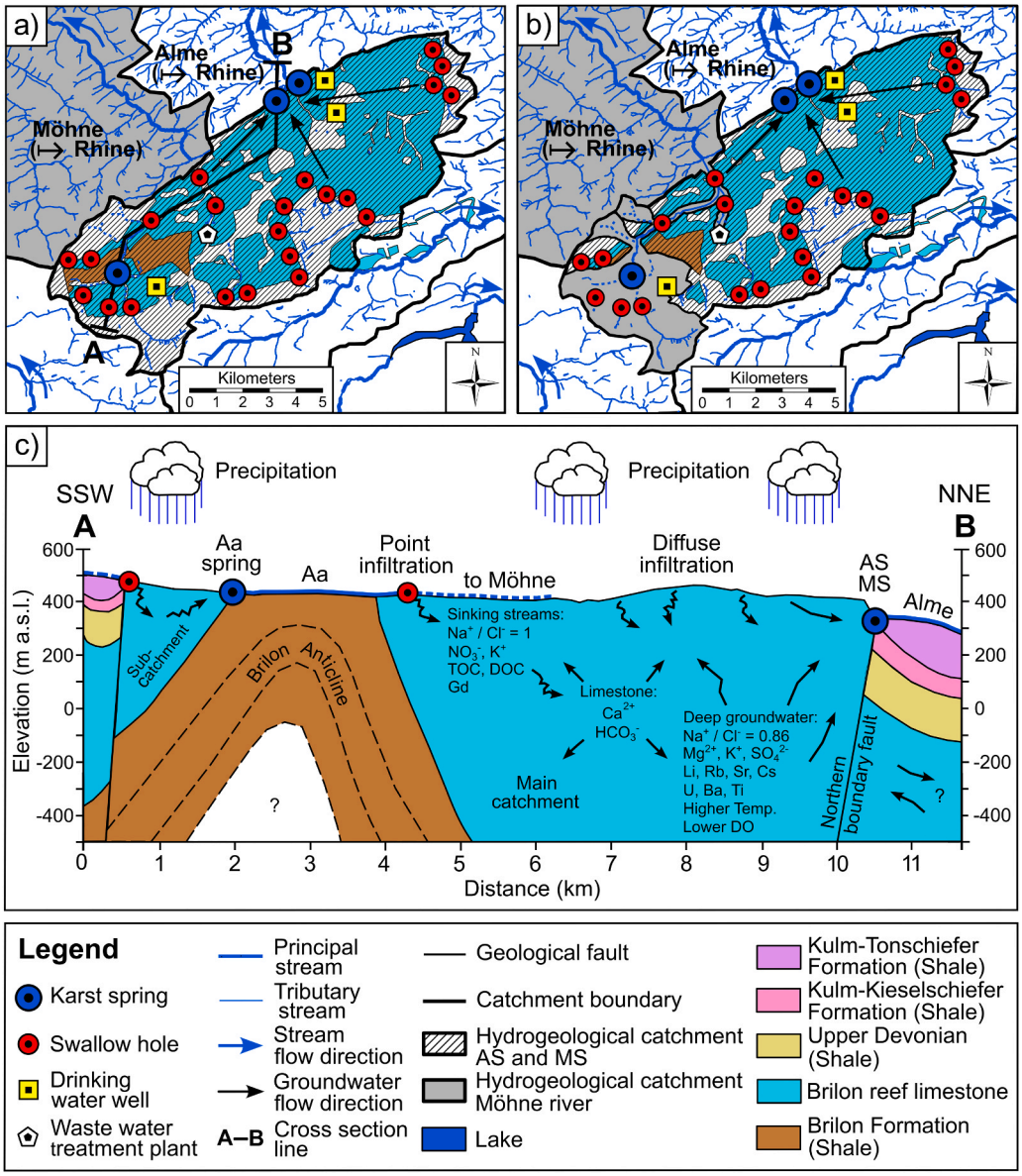

Fig. 15. Catchment area of AS and MS depending on the current hydrological conditions. Base map: Geological Service NRW (2024). a) Complete sinking of surface water at the Aa and Möhne swallow holes. b) No sinking of surface water at the Aa and Möhne swallow holes. c) Hydrogeological conceptual model of the BKS, profile line is shown in a).

Sampling sites with low or no influence of the deeper groundwater are suitable (e.g. AS 3, Karst DWW 2–3). Furthermore, investigations including stable isotopes (^{18}O and ^{2}H) are suitable to identify possible surface-subsurface interactions during a specific rainfall event, and to determine mean residence times (Diamond, 2022). The mean residence time of 30–50 years of the deeper karst groundwater stated by Koch (1998) should be re-examined and updated with the current state of the art. A continuous monitoring at the swallow holes of the WWIS should be established to improve the knowledge on anthropogenic contaminants infiltrating into the BKS. To quantify the input of critical parameters such as NO_3^-, all sinking streams ending in swallow holes (Fig. 1b) should be regularly monitored. Currently, long-term data are only available for the drinking water abstraction sites. Such data should be generated for the main karst springs, AS and MS, too, with a particular regard to the trace elements correlating with Cl^-. Finally, tracer tests should be conducted to prove connections between swallow holes and springs, DWW, and GMW, and to verify the conceptual model.

5.6. Interconnection of the subcatchment and conceptual model

Groundwater flow directions are directed from the swallow holes to the karst springs (Fig. 1c). Aa and Möhne surface waters sinking into the BKS are expected to flow in a northeasterly direction toward AS and MS. Since the subcatchment is drained by the Aa spring/stream, swallow holes in Aa and Möhne play an important role for the interconnection with the main catchment. Depending on the current hydrological status, the subcatchment is fully or only partly connected with the main catchment. In periods when all of the Aa surface water sinks into the BKS via swallow holes, the subcatchment is fully connected to the main catchment (Fig. 15a). In periods when the swallow holes cannot absorb all of the water, the Aa continues to flow on the surface and is led out of the BKS via the Möhne (Fig. 15b). In this case, the hydrogeological catchment of AS and MS is thus smaller. Two endpoints can be defined. Full sinking at the swallow holes, this status occurs in summer and autumn times. The second endpoint would be reached when all the Aa water flows over the swallow holes with no sinking into the karst system at all. However, the second endpoint likely never occurs in nature, as some water always sinks into the aquifer via the swallow holes. In periods when parts of the Aa water flow to the Möhne, and parts sink into the BKS, the subcatchment is thus partially disconnected from the main catchment. The hydrogeological conceptual model summarizes the findings of this study (Fig. 15c) and depicts the interconnection of the subcatchment with the main catchment via the Aa spring and swallow holes in the Aa stream. Main hydrochemical findings are shown with the duality between signals coming from the surface and the deeper groundwater. The deeper groundwater is absent in the subcatchment. Contaminants present in the subcatchment can transfer into the main catchment. Hence, water protection actions must always consider the whole hydrogeological catchment area, including the subcatchment.

6. Conclusions

This study develops the first comprehensive hydrogeological and hydrochemical conceptual model of the deep Brilon karst system (BKS). The compilation of data from springs, drinking water wells (DWW), groundwater monitoring wells (GMW), and surface streams generated an abundant dataset that allowed for the first time to thoroughly evaluate the hydrochemical characteristics at different spatial and temporal scales. The BKS is a deep carbonate rock aquifer, mostly fractured, and only moderately karstified.

Main findings are:

(1) The BKS is characterized by strong spatial variations at both spring and catchment scale. Strongest variations are found for Na^+ and Cl^- related with deeper groundwater, Cl^- concentrations vary by a factor of 34. The deeper groundwater is distinctly present in individual sampling sites with varying quantities. Na^+ and Cl^- concentrations are comparatively low in the subcatchment. Compared with the karst springs and DWW, some karst GMW show significantly higher Ca^{2+} and HCO_3^- concentrations.
(2) Karst groundwater samples show Na^+/Cl^- ratios of 0.86 resulting from the dissolution of evaporites, whereas the Na^+ and Cl^- concentrations of the waste water influenced stream (WWIS) and surface streams originate from the application of road salt with a Na^+/Cl^- ratio of about 1. For the karst groundwater, Cl^- correlates positively with most other major ions (with exception of NO_3^-) and the trace elements Li, Rb, Sr, Cs, U, Ba, and Ti. Negative correlations are found with NO_3^- and DO. For the WWIS and surface streams, Cl^- correlates positively with NO_3^-, TOC, DOC, and Gd, among other parameters.
(3) The karst groundwater is characterized by low seasonal hydrochemical variations with no direct impact from sinking streams and the WWIS, whereas the karst spring discharge shows clear seasonal variations with highest discharge in spring and lowest discharge in autumn. The deeper groundwater is mostly uncoupled from influences coming from the surface.
(4) Long-term data of MS 4 and Karst DWW 1–2 show significantly increasing trends of Ca^{2+}, Mg^{2+}, Na^+, and Cl^- concentrations, associated with a growing influence of the deeper groundwater. In contrast, long-term NO_3^- concentrations are significantly decreasing or stable at these sampling sites.

The study not only provides new hydrological insights for the BKS, but also addresses and expands the knowledge on deep karst aquifer systems in general. Future research dealing with such systems can make use of the findings.

CRediT authorship contribution statement

Nadine Goeppert: Writing – review & editing, Supervision, Project administration, Methodology, Funding acquisition, Formal analysis, Conceptualization. **Nico Goldscheider:** Writing – review & editing, Supervision, Project administration, Methodology, Funding acquisition, Formal analysis, Conceptualization. **Alexander Kaltenbrunn:** Writing – review & editing, Writing – original

draft, Visualization, Software, Methodology, Formal analysis, Data curation, Conceptualization.

Declaration of Competing Interest

The authors declare that they have no known competing financial interests or personal relationships that could have appeared to influence the work reported in this paper.

Acknowledgments

This work was supported by the Stadtwerke Brilon (Brilon municipal utilities), as well as by the European Confederation of Upper-Rhine Universities (EUCOR) in the framework of the MOKA project (Molecular ecology of karst springs), funded as part of the Excellence Strategy of the German Federal and State Governments. The authors would like to thank the Stadtwerke Brilon for the logistical help, for providing access to the drinking water facilities during the sampling campaigns in the years 2020 and 2021 and for providing hydrochemical data from the drinking water abstraction sites. Special thanks are given to Ariane Detering for the help in the field during the sampling campaigns in December 2020, January and March 2021. Further thanks go to the KIT laboratory staff Christine Roske-Stegemann, Daniela Blank and Chris Buschhaus.

Appendix A. Supporting information

Supplementary data associated with this article can be found in the online version at doi:10.1016/j.ejrh.2026.103473.

Data availability

Hydrochemical data collected in the course of the six sampling campaigns are available via a HydroShare repository (https://doi.org/10.4211/hs.c2797acb6ed7433ab93b794cee5e6880). The OpenGeodata.NRW datasets are publicly and freely available, links are given in the References. Hydrochemical data from the Brilon municipal utilities is available from the corresponding author upon reasonable request.

References

[dataset] OpenGeodata.NRW, 2025a. Grundwassermessstellen NRW [Groundwater monitoring wells NRW]. ⟨https://www.opengeodata.nrw.de/produkte/umwelt_klima/wasser/grundwasser/hygrisc/⟩. Accessed 21 October 2025.

[dataset] OpenGeodata.NRW, 2025b. GÜS Messstellen Chemie NRW [Water monitoring system chemistry NRW]. ⟨https://www.opengeodata.nrw.de/produkte/umwelt_klima/wasser/oberflaechengewaesser/gues/⟩. Accessed 21 October 2025.

[dataset] OpenGeodata.NRW, 2025c. Geprüfte Zeitreihen der Abflüsse [Audited discharge time series]. ⟨https://www.opengeodata.nrw.de/produkte/umwelt_klima/wasser/oberflaechengewaesser/hydro/q/⟩. Accessed 21 October 2025.

Alijani, F., Bayat, N., Nassery, H.R., Lorenz, G.D., Heine, F., Leybourne, M.I., 2025. Insights into groundwater hydrochemistry and origin of the hydrocarbon contaminated karst aquifers, SW Iran. J. Hydrol. Reg. Stud. 59, 102379. https://doi.org/10.1016/j.ejrh.2025.102379.

Bakalowicz, M., 2005. Karst groundwater: a challenge for new resources. Hydrogeol. J. 13, 148–160. https://doi.org/10.1007/s10040-004-0402-9.

Bao, Y., Pang, Z., Huang, T., Li, Y., Tian, L., Luo, J., Qian, T., 2022. Chemical and isotopic evidences on evaporite dissolution as the origin of high sulfate water in a karst geothermal reservoir. Appl. Geochem. 145, 105419. https://doi.org/10.1016/j.apgeochem.2022.105419.

Bau, M., Schmidt, K., Pack, A., Bendel, V., Kraemer, D., 2018. The European Shale: an improved data set for normalisation of rare earth element and yttrium concentrations in environmental and biological samples from Europe. Appl. Geochem. ICS 90 (1), 142–149. https://doi.org/10.1016/j.apgeochem.2018.01.008.

Bauer, J., Börsig, N., Pham, V.C., Hoan, T.V., Ngyuen, H.T., Norra, S., 2022. Geochemistry and evolution of groundwater resources in the context of salinization and freshening in the southernmost Mekong Delta, Vietnam. J. Hydrol. Reg. Stud. 40. https://doi.org/10.1016/j.ejrh.2022.101010.

Bezirksregierung Köln , 2024a. Topographical map of NRW 1:10,000, ⟨https://www.opengeodata.nrw.de/produkte/geobasis/tk/akt/dtk10nrw/dtk10nrw_farbe_tiff/⟩. Accessed November 2024.

Bezirksregierung Köln , 2024b. Amtliche Basiskarte NRW [Official base map NRW], ⟨https://www.opengeodata.nrw.de/produkte/geobasis/lk/akt/abk_tiff/abk_sw_tiff/⟩. Accessed November 2024.

Black, T.J., 2012. Deep karst system research, Michigan, USA. Carbonates Evaporites 27, 119–122. https://doi.org/10.1007/s13146-012-0093-6.

Boester, U., Rüde, T.R., 2020. Utilize gadolinium as environmental tracer for surface water-groundwater interaction in Karst. J. Contam. Hydrol. 235, 103710. https://doi.org/10.1016/j.jconhyd.2020.103710.

Bonacci, O., 2015. Chapter 5 Surface Waters and Groundwater in Karst. In: Stevanović, Z. (Ed.), Karst Aquifers-Characterization and Engineering. Professional Practice in Earth Sciences. Springer, Cham, pp. 149–169. https://doi.org/10.1007/978-3-319-12850-4_5.

Brünjes, R., Hofmann, T., 2020. Anthropogenic gadolinium in freshwater and drinking water systems. Water Res. 182, 115966. https://doi.org/10.1016/j.watres.2020.115966.

Carucci, V., Petitta, M., Aravena, R., 2012. Interaction between shallow and deep aquifers in the Tivoli Plain (Central Italy) enhanced by groundwater extraction: A multi-isotope approach and geochemical modeling. Appl. Geochem. 27 (1), 266–280. https://doi.org/10.1016/j.apgeochem.2011.11.007.

Chen, Z., Auler, A.S., Bakalowicz, M., Drew, D., Griger, F., Hartmann, J., Jiang, G., Moosdorf, N., Richts, A., Stevanović, Z., Veni, G., Goldscheider, N., 2017. The World Karst Aquifer Mapping project: concept, mapping procedure and map of Europe. Hydrogeol. J. 25, 771–785. https://doi.org/10.1007/s10040-016-1519-3.

Diamond, R.E., 2022. Stable Isotope Hydrology. The Groundwater Project, Guelph, Ontario, Canada. https://doi.org/10.21083/978-1-77470-043-3.

DIN 38402-62, 2014. German standard methods for the examination of water, waste water and sludge - General information (group A) - Part 62: Plausibility check of analytical data by performing an ion balance. Beuth Verlag GmbH, Berlin.

Drever, J.I., 1997. The geochemistry of natural waters. Surface and groundwater environments. Third edition. The groundwater project. ⟨https://gw-project.org/books/the-geochemistry-of-natural-waters/⟩.

Ebrahimi, P., Barbieri, M., 2019. Gadolinium as an Emerging Microcontaminant in Water Resources: Threats and Opportunities. Geosciences 9 (2), 93. https://doi.org/10.3390/geosciences9020093.

European Union, 2020. Directive 2020/2184 of the European Parliament and of the Council of 16 December 2020 on the quality of water intended for human consumption (recast).
Fernández-Ortega, J., Barberá, J.A., Andreo, B., 2023. Coupling major ions and trace elements to turbidity dynamics for allogenic contribution assessment in a binary karst system (Sierra de Ubrique, S Spain). Environ. Earth Sci. 82, 536. https://doi.org/10.1007/s12665-023-11227-0.
Ford, D., Williams, P., 2007. Karst Hydrogeology and Geomorphology. John Wiley and Sons, Ltd.
Frank, S., Fahrmeier, N., Goeppert, N., Goldscheider, N., 2022. High-resolution multi-parameter monitoring of microbial water quality and particles at two alpine karst springs as a basis for an early-warning system. Hydrogeol. J. 30, 2285–2298. https://doi.org/10.1007/s10040-022-02556-8.
Geological Service NRW, 2024. Geological map of NRW 1:100,000. ⟨https://www.opengeodata.nrw.de/produkte/geologie/geologie/GK/ISGK100/ISGK100vektor/⟩. Accessed Nov 2024.
German Meteorological Service, 2026. Daily station data. ⟨https://cdc.dwd.de/portal/⟩. Accessed Jan 2026.
Ghasemizadeh, R., Hellweger, F., Butscher, C., Padilla, I., Vesper, D., Field, M., Alshawabkeh, A., 2012. Review: Groundwater flow and transport modeling of karst aquifers, with particular reference to the North Coast Limestone aquifer system of Puerto Rico. Hydrogeol. J. 20, 1441–1461. https://doi.org/10.1007/s10040-012-0897-4.
Gil-Márquez, J.M., Andreo, B., Mudarra, M., 2019. Combining hydrodynamics, hydrochemistry, and environmental isotopes to understand the hydrogeological functioning of evaporite-karst springs. An example from southern Spain. J. Hydrol. 576, 299–314. https://doi.org/10.1016/j.jhydrol.2019.06.055.
Göb, S., Loges, A., Nolde, N., Bau, M., Jacob, D.E., Markl, G., 2013. Major and trace element compositions (including REE) of mineral, thermal, mine and surface waters in SW Germany and implications for water–rock interaction. Appl. Geochem. 33, 127–152. https://doi.org/10.1016/j.apgeochem.2013.02.006.
Goldscheider, N., 2015. Chapter 4 Overview of Methods Applied in Karst Hydrogeology. In: Stevanović, Z. (Ed.), Karst Aquifers—Characterization and Engineering. Professional Practice in Earth Sciences. Springer, Cham, pp. 127–145. https://doi.org/10.1007/978-3-319-12850-4_4.
Goldscheider, N., Drew, D., Worthington, S., 2007. Chapter 1 Introduction. In: Goldscheider, N., Drew, D. (Eds.), Methods in karst hydrogeology. Taylor and Francis, Leiden; New York, pp. 1–8. https://doi.org/10.1201/9781482266023.
Gong, W., Zang, C., Ma, J., Sun, Y., Zhang, H., Xu, P., Jiang, M., 2025. Hydrochemical characteristics and controlling factors of deep karst groundwater in Huaibei Plain, Huaihe River Basin, China. Front. Earth Sci. 13. https://doi.org/10.3389/feart.2025.1552125.
Grobe, M., Machel, H.G., 2002. Saline groundwater in the Muensterland Cretaceous Basin, Germany: clues to its origin and evolution. Mar. Pet. Geol. 19 (3), 307–322. https://doi.org/10.1016/S0264-8172(02)00019-3.
Guo, Y., Zhang, F., Zhang, N., Liu, Y., Xiao, Q., Feng, Y., Chen, H., 2025. Hydrogeological characteristics and hydro-chemical environment of a karst aquifer system are determined by the presence of major ions, trace elements, and environmental isotopes. Water Res. X 28, 100377. https://doi.org/10.1016/j.wroa.2025.100377.
Hamdan, I., Licha, T., Toll, M., Margane, A., Sauter, M., 2020. Quantification of wastewater pollution load using potassium concentrations in karst spring discharges. Environ. Earth Sci. 79, 402. https://doi.org/10.1007/s12665-020-09145-6.
Haryono, E., 2023. Advances in Karst Geomorphology and Hydrogeology Research in the Last Decade and Its Future Direction for Karst Land Use Planning. In: Bański, J., Meadows, M. (Eds.), Research Directions, Challenges and Achievements of Modern Geography. Advances in Geographical and Environmental Sciences. Springer, Singapore, pp. 231–253. https://doi.org/10.1007/978-981-99-6604-2_12.
Heuer, F., Korn, D., Belka, Z., Hairapetian, V., 2015. Facies, origin, and palaeontological inventory of an Early Carboniferous neptunian dyke in the Devonian reef limestone near Rösenbeck (Brilon Anticline, Rhenish Mountains). Foss. Rec. 18, 57–72. https://doi.org/10.5194/fr-18-57-2015.
Heuser, H., 2017. Grundwasser. [Groundwater]. In. Geologie im Rheinischen Schiefergebirge. Teil 3: Sauer- und Siegerland. Geological Service NRW, Krefeld, pp. 169–184. ⟨https://www.gd.nrw.de/pdf/geologie-sauer-siegerland-rsg3.pdf⟩.
Hölting, B., Coldewey, W., 2019. Hydrogeology. Springer Textbooks in Earth Sciences, Geography and Environment. Springer Berlin, Heidelberg. https://doi.org/10.1007/978-3-662-56375-5.
Huebsch, M., Fenton, O., Horan, B., Hennessy, D., Richards, K.G., Jordan, P., Goldscheider, N., Butscher, C., Blum, P., 2014. Mobilisation or dilution? Nitrate response of karst springs to high rainfall events. Hydrol. Earth Syst. Sci. 18, 4423–4435. https://doi.org/10.5194/hess-18-4423-2014.
Hunkeler, D., Mudry, J., 2007. Chapter 6 Hydrochemical methods. In: Goldscheider, N., Drew, D. (Eds.), Methods in karst hydrogeology. Taylor and Francis, Leiden; New York, pp. 93–121. https://doi.org/10.1201/9781482266023.
Johannesson, K.H., Stetzenbach, K.J., Hodge, V.F., Kreamer, D.K., Zhou, X., 1997. Delineation of Ground-Water Flow Systems in the Southern Great Basin Using Aqueous Rare Earth Element Distributions. Groundwater 35, 807–819. https://doi.org/10.1111/j.1745-6584.1997.tb00149.x.
Jones, B.F., Vengosh, A., Rosenthal, E., Yechieli, Y., 1999. Chapter 3: Geochemical Investigations. In: Bear, J., Cheng, A.H.D., Sorek, S., Ouazar, D., Herrera, I. (Eds.), Seawater Intrusion in Coastal Aquifers — Concepts, Methods and Practices. Theory and Applications of Transport in Porous Media, 14. Springer, Dordrecht, pp. 51–71. https://doi.org/10.1007/978-94-017-2969-7_3.
Kaltenbrunn, A., Goeppert, N., Goldscheider, N., 2026. Hydrochemical data from a deep karst aquifer system. HydroShare, Brilon, Germany. https://doi.org/10.4211/hs.c2797acb6ed7433ab93b794cee5e6880.
Kilchmann, S., Waber, H.N., Parriaux, A., Bensimon, M., 2004. Natural tracers in recent groundwaters from different Alpine aquifers. Hydrogeol. J. 12, 643–661. https://doi.org/10.1007/s10040-004-0366-9.
Koch, M., 1998. Die Almequellen. [The Alme springs]. In: Erläuterungen zu Blatt C 4714 Arnsberg. Geological map of NRW 1:100,000. 2. Auflage. Geological Service NRW, Krefeld, pp. 57–61. ⟨https://www.opengeodata.nrw.de/produkte/geologie/geologie/GK/ISGK100/GK100analog/GK100-C4714-Arnsberg_EPSG25832_JPEG.zip⟩.
Koch, M., Vogel, K., 1992. Der Almeteich bei Brilon/Alme (Hochsauerlandkreis) - ein Beitrag zur Hydrogeologie des Briloner Massenkalks. [The Alme spring pond in Brilon/Alme (High Sauerland District) - a contribution to the hydrogeology of the Brilon reef limestone]. Stadt Brilon, Brilon.
Kpegli, K.A.R., Alassane, A., van der Zee, S.E.A.T.M., Boukari, M., Mama, D., 2018. Development of a conceptual groundwater flow model using a combined hydrogeological, hydrochemical and isotopic approach: a case study from southern Benin. J. Hydrol. Reg. Stud. 18, 50–67. https://doi.org/10.1016/j.ejrh.2018.06.002.
Kuniansky, E.L., Taylor, C.J., Williams, J.H., Paillet, F., 2022. Introduction to Karst Aquifers. The Groundwater Project. https://doi.org/10.21083/978-1-77470-040-2.
Mahler, B.J., Valdes, D., Musgove, M., Massei, N., 2008. Nutrient dynamics as indicators of karst processes: Comparison of the Chalk aquifer (Normandy, France) and the Edwards aquifer (Texas, U.S.A.). J. Contam. Hydrol. 98 (s 1-2), 36–49. https://doi.org/10.1016/j.jconhyd.2008.02.006.
McLennan, S.M., 2001. Relationships between the trace element composition of sedimentary rocks and upper continental crust. Geochem Geophys Geosyst 2, 2000GC000109. https://doi.org/10.1029/2000GC000109.
Merk, M., Goeppert, N., Goldscheider, N., 2020. Processes controlling spatial and temporal dynamics of spring water chemistry in the Black Forest National Park. Sci. Total Environ. 723, 137742. https://doi.org/10.1016/j.scitotenv.2020.137742.
Milanović, S., Vasić, L., 2015. Chapter 12 Monitoring of Karst Groundwater. In: Stevanović, Z. (Ed.), Karst Aquifers—Characterization and Engineering. Professional Practice in Earth Sciences. Springer, Cham, pp. 335–359. https://doi.org/10.1007/978-3-319-12850-4_12.
Möller, D., 1990. The Na/Cl ratio in rainwater and the seasalt chloride cycle. Tellus B. Chem. Phys. Meteorol. 42 (3), 254–262. https://doi.org/10.1034/j.1600-0889.1990.t01-1-00004.x.
Mueller, Y.K., Goeppert, N., Goldscheider, N., 2025. Transferring the paired-catchment approach to the subsurface: new insights into the transport and spatiotemporal dynamics of contaminants in an active karst conduit system. Hydrogeol. J. 33, 1825–1847. https://doi.org/10.1007/s10040-025-02962-8.
Nordstrom, D.K., Plummer, L.N., Wigley, T.M., Wolery, T.H., Ball, J.W., Jenne, E.A., Bassett, R.L., Crerar, D.A., Florence, T.M., Fritz, B., Hoffman, M., Holdren, G.R., Lafon, G.M., Mattigod, S.V., McDuff, R.E., Morel, F., Reddy, M.M., Sposito, G., Thrailkill, J., 1979. A comparison of computerized chemical models for equilibrium calculations in aqueous systems. In: Jenne, E. (Ed.), Chemical modeling in aqueous systems, speciation, sorption, solubility, and kinetics. American Chemical Society, pp. 857–892. https://doi.org/10.1021/bk-1979-0093.ch038.
Panno, S.V., Hackley, K.C., Hwang, H.H., Greenberg, S.E., Krapac, I.G., Landsberger, S., O'Kelly, D.J., 2006. Characterization and Identification of Na-Cl Sources in Ground Water. Groundwater 44 (2), 176–187. https://doi.org/10.1111/j.1745-6584.2005.00127.x.

Pas, D., Da Silva, A.C., Cornet, P., Bultynck, P., Königshof, P., Boulvain, F., 2013. Sedimentary development of a continuous Middle Devonian to Mississippian section from the fore-reef fringe of the Brilon Reef Complex (Rheinisches Schiefergebirge, Germany. Facies 59, 969–990. https://doi.org/10.1007/s10347-012-0351-z.

Pujades-Garnes, E., Ekiz, M.Ç., Izquierdo, M., Scheiber, L., Siavashani, N.S., Juradi, A., Vazquez-Sune, E., Foppen, J.W., 2025. Behaviour and Fate of Anthropogenic Gadolinium in Groundwater: Insights from Batch Experiments and Measured Concentrations in the Besòs River Delta (NE Spain). Environ. Process 12, 43. https://doi.org/10.1007/s40710-025-00784-0.

Pulido-Bosch, A., 2021. Principles of Karst Hydrogeology. Conceptual Models, Time Series Analysis, Hydrogeochemistry and Groundwater Exploitation. Springe Textb. Earth Sci. Geogr. Environ. https://doi.org/10.1007/978-3-030-55370-8.

Schmidt, K., Bau, M., Merschel, G., Tepe, N., 2019. Anthropogenic gadolinium in tap water and in tap water-based beverages from fast-food franchises in six major cities in Germany. Sci. Total Environ. 687, 1401–1408. https://doi.org/10.1016/j.scitotenv.2019.07.075.

Spellman, P., Pain, A., Breithaupt, C., Bremner, P.M., 2024. Using multivariate statistics to link major ion chemistry changes at karst springs to agriculture. Sci. Total Environ. 921, 170573. https://doi.org/10.1016/j.scitotenv.2024.170573.

Stevanović, Z., 2019. Karst waters in potable water supply: a global scale overview. Environ. Earth Sci. 78, 662. https://doi.org/10.1007/s12665-019-8670-9.

Stevanović, Z., Gunn, J., Goldscheider, N., Ravbar, N., 2024. Karst: Environment and management of aquifers. The Groundwater Project, Guelph, Ontario, Canada. https://doi.org/10.62592/AWCU2984.

Stichling, S., Becker, R.T., Hartenfels, S., Aboussalam, Z.S., May, A., 2022. Drowning, extinction, and subsequent facies development of the Devonian Hönne Valley Reef (northern Rhenish Massif, Germany). Palaeobio Palaeoenv 102, 629–696. https://doi.org/10.1007/s12549-022-00539-x.

Stober, I., 2014. Hydrochemical properties of deep carbonate aquifers in the SW German Molasse basin. Geotherm. Energy 2, 13. https://doi.org/10.1186/s40517-014-0013-1.

Strebel, O., Duynisveld, W.H.M., Böttcher, J., 1989. Nitrate Pollution of Groundwater in Western Europe. Agric. Ecosyst. Environ. 26, 189–214. https://doi.org/10.1016/0167-8809(89)90013-3.

Subyani, A.M., Şen, Z., 2006. Refined chloride mass-balance method and its application in Saudi Arabia. Hydrol. Process 20 (20), 4373–4380. https://doi.org/10.1002/hyp.6172.

Tepe, N., Romero, M., Bau, M., 2014. High-technology metals as emerging contaminants: Strong increase of anthropogenic gadolinium levels in tap water of Berlin, Germany, from 2009 to 2012. Appl. Geochem. 45, 191–197. https://doi.org/10.1016/j.apgeochem.2014.04.006.

Toth, D., Katz, B., 2006. Mixing of shallow and deep groundwater as indicated by the chemistry and age of karstic springs. Hydrogeol. J. 14, 1060–1080. https://doi.org/10.1007/s10040-006-0099-z.

Tran, D.A., Goeppert, N., Goldscheider, N., 2023. Use of major ion chemistry and trace and rare earth elements to characterize hydraulic relations, mixing processes and water–rock interaction in the Dong Van karst aquifer system, Northern Vietnam. Hydrogeol. J. 31, 1735–1753. https://doi.org/10.1007/s10040-023-02689-4.

Wang, L., Xiao, Y., Yang, H., Zhang, Y., Wang, S., Qi, Z., Han, J., Hu, W., Wang, J., Hao, Q., Senapthi, V., 2024. Formation mechanism of high-altitude glacial mineral water in the Kunlun Mountains of Tibetan Plateau: Insights from isotopes and hydrochemistry. J. Hydrol. Reg. Stud. 53, 101789. https://doi.org/10.1016/j.ejrh.2024.101789.

Ward, J.H., 1963. Hierarchical Grouping to Optimize an Objective Function. J. Am. Stat. Assoc. 58, 236–244. https://doi.org/10.1080/01621459.1963.10500845.

White, W.B., 1999. Chapter 18 Groundwater flow and transport in karst. In: Delleur, J.W. (Ed.), The Handbook of Groundwater Engineering. CRC Press, pp. 687–722. ⟨http://amac.md/Biblioteca/data/28/14/10/23.2.pdf⟩.

WHO, 2022. Guidelines for drinking water quality, fourth edition incorporating the first and second addenda. ⟨https://www.who.int/publications/i/item/9789240045064⟩. Accessed December 2025.

Williams, L.J., Kuniansky, E.L., 2016. Revised hydrogeologic framework of the Floridan aquifer system in Florida and parts of Georgia, Alabama, and South Carolina. U.S. Geological Survey Professional Paper 1807. https://doi.org/10.3133/pp1807.

Wu, X., Li, C., Sun, B., Geng, F., Gao, S., Lv, M., Ma, X., Li, H., Xing, L., 2020. Groundwater hydrogeochemical formation and evolution in a karst aquifer system affected by anthropogenic impacts. Environ. Geochem Health 42, 2609–2626. https://doi.org/10.1007/s10653-019-00450-z.

Zwahlen, F., 2004. Vulnerability and risk mapping for the protection of carbonate (karst) aquifers. Eur. Comm. COST-Action 620. ⟨https://op.europa.eu/en/publication-detail/-/publication/be3c99bf-1a0a-4213-b35d-c3faffcd355b/language-en⟩.